Author/s:
Li, M;Wang, H;Luo, W;Sherrell, PC;Chen, J;Yang, J

Title:
Heterogeneous Single-Atom Catalysts for Electrochemical CO2 Reduction Reaction

Date:
2020-08-27

Citation:
Li, M., Wang, H., Luo, W., Sherrell, P. C., Chen, J. & Yang, J. (2020). Heterogeneous Single-Atom Catalysts for Electrochemical CO2 Reduction Reaction. Advanced Materials, 32 (34), https://doi.org/10.1002/adma.202001848.

Persistent Link:
https://hdl.handle.net/11343/275998

WILEY-VCH

Heterogeneous Single-Atom Catalysts for Electrochemical CO_2 Reduction Reaction

Minhan Li, Haifeng Wang, Wei Luo, Peter C. Sherrell, Jun Chen* and Jianping Yang**

M. H. Li, H. F. Wang, Prof. W. Luo, Prof. J. P. Yang

State Key Laboratory for Modification of Chemical Fibers and Polymer Materials, International Joint Laboratory for Advanced Fiber and Low-dimension Materials, College of Materials Science and Engineering, Donghua University, Shanghai 201620, P. R. China

E-mail: wluo@dhu.edu.cn; jianpingyang@dhu.edu.cn

Dr P. C. Sherrell

Department of Chemical Engineering, The University of Melbourne, Parkville, VIC 3010, Australia

Prof. J. Chen

ARC Centre of Excellence for Electromaterials Science, Intelligent Polymer Research Institute, Australian Institute of Innovative Materials, Innovation Campus

University of Wollongong, Wollongong, NSW 2522, Australia

Email: junc@uow.edu.au

Keywords: CO_2 reduction reaction, electrocatalyst, single-atom catalysts, N-doped carbon, metal-nitrogen sites

Abstract: The electrochemical CO_2 reduction reaction (CO_2RR) is of great importance to tackle the rising CO_2 concentration in the atmosphere. The CO_2RR can be driven by renewable energy sources, producing precious chemicals and fuels, with the implementation of this process largely relying on the development of low-cost and efficient electrocatalysts. Recently, a range of heterogeneous, potentially low cost, single-atom catalysts (SACs) containing non-precious metals coordinated to earth-abundant elements, such as C, N, O and S, have emerged as promising candidates for the CO_2RR. A variety of products including formic acid, ethylene, ethanol, and n-propanol, have been produced on different SACs however carbon monoxide (CO) as remains the predominant reduction product. Unfortunately, the real catalytically active centers and the key factors that govern the catalytic performance of these SACs remain ambiguous. This review focuses

on addressing this ambiguity by developing a fundamental understanding of the CO_2RR-to-CO on SACs, as CO accounts for the major product from CO_2RR on SACs. The reaction mechanism, the rate-determining steps, and the crucial factors that control the activity and selectivity of SACs are analyzed from both experimental and theoretical studies. Then, the synthesis, characterization, and the CO_2RR to CO performance of SACs are discussed. Finally, the challenges are highlighted and future pathways proposed in the hope of guiding the design of the SACs to promote and understand the CO_2RR on SACs.

1 Introduction

Carbon dioxide (CO_2) is a notorious greenhouse gas, causing an increase in global average temperature, changes in climate, ocean acidification and the disruption of carbon cycle in nature. The global average CO_2 concentration in the atmosphere has reached an unprecedented level for modern times of 405 ppm in 2017, which is higher than at any point in the past 800,000 years.[1-3] The task to reduce the CO_2 concentration in the atmosphere is so urgent that, according to the Intergovernmental Panel on Climate Change (IPCC), the net anthropogenic CO_2 emission needs to be reduced to zero by 2050 to limit the global warming to the critical 1.5 °C above pre-industrial levels.[4] With the continual economic demand for devices that produce CO_2 emissions and ever increasing global energy consumption, to significantly reduce the CO_2 level in the atmosphere and utilize it in an efficient way are pressing and important grand research challenges.[5-7] Different approaches have been proposed to address the CO_2 issue: to improve the combustion efficiency of fossil fuels, to physically capture and store CO_2, and to chemically convert CO_2 into useful chemicals.[8-9] However, only the approach that is capable of both mitigating the CO_2 emission and supplying sustainable energy to society is the electrochemical CO_2 reduction reaction (CO_2RR).[7, 10-11] Further, this approach enables valorization of CO_2 into useful chemicals.

The CO_2 molecule can be converted into useful chemicals via chemical conversion,[12-13] biological transformation,[14] photocatalytic,[15-16] and electrocatalytic reduction. In recent years, the CO_2RR has emerged as the most promising due to its intriguing advantages: 1) the electricity, the driving force that reduces CO_2 to multiple valuable products, can come from renewable but intermittent energy sources, such as solar, wind, tidal, or geothermal power; 2) the products from the electrochemical CO_2RR , including carbon monoxide, formate acid, acetate, hydrocarbons (methane, ethene, ethane, etc.) and alcohols (methanol, ethanol, n-propanol, etc.), are either fuels or important chemicals that fit into the existing vehicles and industries; 3) the controllable process and mild reaction conditions; 4) the electrocatalysis systems are simple and easy to scale-up. For instance, combined with gas diffusion electrodes (GDE) and flow-cell configurations, high current densities (200-600 mA/cm^2) for CO_2RR have been achieved.[17-22] However, the CO_2RR process is

still hampered by the lack of efficient electrocatalysts, presenting low energy efficiency and reaction rate and poor selectivity toward deep reduced products.

Thermodynamically, the half-cell reduction potentials of CO_2 to the main products (listed above) are within ±0.2 V of hydrogen evolution reaction (HER) (**Error! Reference source not found.**a). However, the high CO_2 activation barrier and reaction pathways that involve multiple electron transfer steps result in the sluggish kinetics for CO_2RR, showing high overpotentials and poor selectivity.[11, 23] Therefore, the CO_2RR processes are largely dependent on the electrocatalysts, which lower the overpotential, accelerate the reaction rates, and improve the selectivity.[24] The CO_2RR electrocatalysts that are widely studied in the literature are metal-organic complexes,[25-26] metal-based materials (including metals, metal oxides, metal alloys, and metal chalcogenides),[23, 27-29] and metal-free carbon-based materials.[9]

Single-atom catalysts featuring isolated metal atoms dispersed on a conductive support have recently become a frontier in catalysis and display exceptional catalytic performance in various processes.[30-34] SACs integrate the advantages of both homogeneous and heterogeneous catalysts. Downsizing the metal sites to atomic scale endows the catalysts with multiple advantages, such as unique electronic structure, low-coordinated metal atoms, strong metal-support interactions, and maximum atom utilization.[35-36] The CO_2 electroreduction over single metal atom sites can be dated back to 1970s when cobalt and nickel phthalocyanines were found to be active for CO_2 electroreduction.[37] Since then, metal-organic complexes with well-defined $M-N_4$ sites have been extensively studied as either homogeneous catalysts or heterogeneous catalysts by immobilizing these molecular catalysts on solid supports through physical adsorption, chemical bonding, polymerization, or integration in frameworks.[26, 38-46] Recently, the use of solid-state heterogeneous SACs containing similar $M-N_x$ moieties for CO_2RR attracts extensive attention because of their facile and flexible preparation methods, unique electronic and geometric structure, outstanding conductivity (especially when supported on carbon materials), great structural stability, and outstanding CO_2RR performance and durability.[31] Even though only 5 years have passed since the first adoption of metal doped nitrogenated carbon as CO_2RR catalysts by Strasser group,[47] the field has developed exceptionally rapidly enabling various single metal sites and different reduction products to be developed and studied (Figure 2). The atomically dispersed metal sites usually act as the main active centers in these catalysts. On the other hand, the coordinated atoms (mostly C and N) around the metal sites are also believed to facilitate the CO_2 activation or the dissociation of the intermediates by electronic polarization.[48-51] The particular synergy in the heterogeneous SACs greatly boosts the catalytic performance of CO_2RR.

There are many excellent reviews focusing on the understanding of the reaction mechanism,[27, 52] the homogeneous and heterogeneous catalysts,[53-54] specific metal-based electrocatalysts,[55-57] and commercial application perspective of CO_2RR process.[58-59] However, only a few reviews have

discussed the application of SACs for CO_2RR. Cheng et al. reported the development of supported SACs for CO_2RR.[60] Yan et al. summarized a variety of CO_2RR catalysts containing M–N_x sites.[61] Varela et al. gave an overall review on the broad CO_2RR catalysts materials containing C, N, and non-precious metals and discussed the active sites and reaction mechanism.[62] Previously, the metal sites in the SACs that were used for CO_2RR were mainly transition metals and CO was the primary reduction product. With the rapid development of this field, more metallic elements dispersed as SACs are emerging and CO_2 reduction products beyond CO are able to be achieved (**Error! Reference source not found.**b). In this context, we focus on the recent development solid-state heterogeneous SACs and highlight their synthetic approaches, characterizations, and the catalytic performance for a variety of products produced over these single sites, even though producing CO_2RR products beyond CO on SACs is still a challenge. Furthermore, we give an insight into the reaction mechanism and the factors that may play a key role in the CO_2RR process. Finally, the challenges and perspectives are put forward for the future research and application of SACs for CO_2RR.

2 Fundamentals of the CO_2RR on SACs

2.1 CO_2 to CO pathway

SACs have recently been extensively studied for CO_2RR due to their outstanding activity and selectivity. The majority of these catalysts produce CO as the main product with excellent performance comparable to traditional noble metal catalysts, such as Au and Ag. Although many works have attempted to understand the reaction pathways and interpret the activity and selectivity trends, the reaction mechanism is still disputed as is the origin of the outstanding catalytic performance.

The proposed mechanisms for CO_2-to-CO on single atom sites often involve the following steps (Figure 3):

(1a) $CO_2 + * + H^+ + e^- \rightarrow * COOH$

(1b) $CO_2 + * + e^- \rightarrow * CO_2^{\cdot -}$

(1c) $* CO_2^{\cdot -} + H^+ \rightarrow * COOH$

(2) $* COOH + H^+ + e^- \rightarrow * CO + H_2O$

(3) $* CO \rightarrow CO + *$

where * denotes the active site on the catalyst surface.

The pathway of CO_2RR to CO via a carboxyl (*COOH) intermediate is widely accepted. The coupled proton–electron transfer (CPET) mechanism is well-established was considered in many studies for CO_2 molecular activation. The CPET mechanism is where a concerted protonation and electron transfer leads to the formation of *COOH from CO_2 (Equation (1a)). The *COOH intermediate then converts to *CO via further proton–electron transfer. Finally, weakly bonded *CO dissociates to generate the CO product. The formation of the Fe–N_4–COOH intermediate from CO_2 via a concerted protonation and electron transfer process has been reported on Fe/NG-750 catalyst with Fe–N_4 moiety.[63] The pathway of CO_2 reduction to CO was also assumed to undergo the coupled proton–electron transfer process to form *COOH and *CO intermediates on Fe– and Co–N_{2+2}–C_8 atomic sites.[51]

On the other hand, a proton decoupled electron transfer mechanism is also brought up, in which the formation of *COOH proceeds in two steps: (1) CO_2 adsorption via one-electron transfer to form an adsorbed $CO_2^{\bullet-}$ (Equation (1b)); and (2) a protonation process of adsorbed $CO_2^{\bullet-}$ intermediate to form *COOH (Equation (1c)). [64–65] The divergence of these two mechanisms lies in whether a $*CO_2^{\bullet-}$ intermediate forms via an electron transfer or *COOH intermediate forms directly via a coupled proton–electron transfer (Figure 3). The reduction of CO_2 on solid Fe–N–C catalyst was proposed to start by forming a (Fe–N–C)–CO_2^- intermediate on the Fe–N sites. This intermediate further underwent a protonation process to form *COOH, which was then reduced to CO.[66] which is consistent with DFT studies and homogeneous molecular catalysts with metal–N macrocyclic complexes.[67–68] By kinetic analysis, the one-electron transfer to CO_2 was also found to be decoupled from a protonation on Fe^{3+}–N–C catalyst.[69] It has also been reported that the CO_2 reduction pathway is also related to the nature of the center metal in the M–N–C catalysts.[70]

With the development and improvement of characterization methods, especially operando spectroscopic techniques, the mechanisms of CO_2RR can be experimentally investigated.[71–72] These include the key intermediates, such as *COOH, *CO, and *CHO, which are detected by in situ attenuated total reflection infrared (ATR-IR) spectroscopy.[73–74] The activation of CO_2 on single Ni atoms which was confirmed by operando X-ray absorption spectroscopy (XAS) and X-ray photoelectron spectroscopy (XPS) techniques.[75] The identification of the key $CO_2^{\bullet-}$ intermediate through *in-situ* FTIR on positively charged single Sn atoms.[76]

2.2 Rate-determining steps (RDSs)

The CO_2 adsorption, *COOH formation and *CO formation would be thermodynamically and kinetically favored with the negatively shifted applied potential.[51, 64] Each of these steps is potentially to be the rate-determining step (RDS) for the overall reaction.

Experimentally, Tafel analysis is a powerful tool to gain insight into the mechanism of electrocatalysis.[77] The calculated Tafel slope, the overpotential divided by the logarithm of the current, provides information crucial to elucidating the rate-determining step (Figure 3). A Fe^{3+}-N-C catalyst showed a Tafel slope of 64-71 mV/dec at low overpotential, indicating the RDS was the protonation of the adsorbed $*CO_2^-$ to form a *COOH intermediate.[69] In another work, Ni-N-C catalyst exhibited a Tafel slope of 118 mV/dec, suggesting a RDS of one-electron transfer to CO_2 to form an adsorbed $*CO_2^{\bullet-}$ intermediate.[70] Graphene supported Ni single atom catalysts also exhibited a Tafel slope of ~110 mV/dec, suggesting the initial CO_2 activation to form *COOH was the RDS.[78] Similar Tafel slopes of 96, 101 and 143 mV/dec also indicated that the first electron transfer step of the *COOH intermediate formation was the RDS, while the lower Tafel slope value attributed to enhanced kinetics of this step.[79] A larger Tafel slope of 194 mV/dec was given by Fe-N-C catalyst, demonstrating the CO_2 adsorption and/or CO desorption is the RDS. Similarly, another Fe-N-C catalyst also exhibited a Tafel slope of 200 mV/dec. However, the formation of *COOH from CO_2 was proposed to be the RDS.[70]

By DFT simulation, the free energy and binding energy of intermediates are commonly used as descriptors to understand the mechanism and interpret the activity and selectivity trends.[80-81] By plotting the free energy diagrams, the formation of *COOH has been considered to be the limiting step on $Fe-N_4$ sites because of a high energy barrier of 0.63 eV.[63] Similarly, based on the calculated free energy diagram, the *COOH formation and the *CO dissociation were identified as the RDS for Ni-N-C and Fe-N-C, respectively.[79] As for Ni/Fe-N-C with Fe-Ni dual sites, the negative free energy of -0.65 eV for *CO indicating the bond between the dual sites and the *CO was so strong that the sites tended to be passivated. However, the barrier for the activation of the second CO_2 molecule was significantly reduced on CO-adsorbed Fe-Ni dual sites, suggesting a different CO_2RR mechanism on atomically dispersed Fe-Ni dual sites.[79]

The RDS for CO_2RR on SACs is related to the nature of the metal center and the applied potentials.[70, 80] Based on the Tafel analysis, Pan et al revealed that the CO_2 reduction proceeded via a rate-limiting one-electron transfer step to CO_2 to form a surface adsorbed $*CO_2^{\bullet-}$ on Ni- and Co-N-C catalysts, while a proton-coupled electron transfer process took place to form a *COOH intermediate as the RDS on Cr-, Mn- and Fe-N-C catalysts.[70] Three overpotential regions were identified by corelating the reaction rate with DFT simulation results. In the low overpotential regime of around -0.45 V_{RHE}, Co-, Fe- and Mn-N-C with relative low binding energy of *COOH presented low onset potentials for CO production. In this regime, the first proton-coupled electron transfer to form *COOH was the potential-determining step. In intermediate overpotential regime of around -0.6 V_{RHE}, the turnover frequency (TOF) of CO showed a great linearity with the *CO binding energy, indicating the rate-determining intermediate has shifted from *COOH to *CO. In

the overpotential regime below -0.7 V_{RHE}, the desorption of CO became the rate-limiting step for Co-, Fe-, and Mn-N-C due to their strong *CO binding strength, while Ni-N-C, which has weak binding of *CO, exhibited a continuous increase in CO production rate with increasing overpotential.[80] Similarly, the decoupled electron transfer step was found to be the rate-determining step for Fe^{2+}-N-C at low overpotential, while CO desorption becoming rate-limiting at high overpotential.[69]

2.3 Effects of the coordination environment around the single atoms

$M-N_x$ moieties are generally believed to play an important role for the CO_2-to-CO activity and CO selectivity in many researches. In contrast to the homogeneous molecular catalysts with well-defined metal-N_4 sites, the coordination environments are complicated in solid-state heterogeneous SACs.[39] Different structures of active sites in solid-state heterogeneous SACs are proposed and present distinct CO_2RR performance.

SACs with porphyrin-like metal-N_4 sites have been extensively predicted to be efficient electrocatalysts for CO_2RR by DFT calculations. [64, 82-84] Experimentally, the local coordination environments of single atom sites are commonly explored by X-ray absorption near edge structure (XANES) and extended X-ray absorption fine structure (EXAFS) spectra. Ni-N_4-C catalyst with an exclusive Ni-N_4 structure produced through a topo-chemical transformation strategy exhibited an accelerated charge transfer rate and a lowered free energy for *COOH formation.[85] Atomic Fe dispersed on N-doped graphene catalysts with Fe-N_4 moieties showed a high FE_{CO} at low overpotential.[63] It was found that nitrogen doping around the Fe-N_4 sites in the graphene matrix changed the free energy for *COOH formation and *CO dissociation, thereby promoting the efficiency of CO_2RR to CO.[63] A Co-N coordination number of 5 was reported on Co-N_5/HNPCSs catalyst. Annealing the catalyst at a moderate temperature (400 and 600 °C) lowered Co-N coordination numbers as well as the FE_{CO}.[86] Pan et al. proposed a unique M-N_4 structure by simulation, where the edge-hosted M-N_{2+2}-C_8 moieties with N atoms from the adjacent graphene layer and C atoms with dangling bonds are more active than the planar M-N_4-C_{10} moieties.[51]

On the other hand, the SACs with favorable low metal-N coordination numbers have also been demonstrated. For instance, a series of C-Zn_xNi_y ZIF-8 catalysts featuring coordinatively unsaturated Ni-N_x sites ($x<3$) showed significantly enhanced CO_2-to-CO activity and CO selectivity compared to the NiPc with well-defined Ni-N_4 sites. DFT calculations revealed that the free energy for *COOH formation was lower on the coordinatively unsaturated Ni-N_x sites than on the Ni-N_4 sites.[87] Heat treatment is an efficient way to regulate the metal-N coordination numbers.[65, 86, 88] The Co-N coordination number decreased from 4.1 to 2.2 with the elevated pyrolysis temperature. The best CO_2RR performance was obtained on the Co-N_2 catalyst that single Co atom coordinated

with two N atoms (Figure 4a).[65] The coordination environments of single Co atom catalysts derived from ZnCo bimetallic MOFs can also be tuned by the pyrolysis temperature. Compared with the $Co_1-N_{4-x}C_x$ catalyst pyrolyzed at 900 ℃, the Co_1-N_4 catalyst pyrolyzed at 800 ℃ exhibited better CO_2RR performance, which may originate from the enhanced CO_2 binding strength caused by the coordination environment of Co.[88]

In addition to coordination numbers, the coordinated N ligands are also critical for CO_2RR on SACs. DFT calculation result revealed that pyrrolic N coordinated Ni (Ni-3N) presented a lower free energy for the formation of *COOH compared to pyridinic N coordinated Ni (Ni-4N) (Figure 4b).[89] Pyrrolic N coordinated atomically dispersed Fe^{3+} ions maintained their initial oxidation state under electrocatalysis conditions at -0.4 V_{RHE} and consequently exhibited outstanding activity and stability, while pyridinic N coordinated Fe^{3+} ions were reduced to Fe^{2+} at -0.1 to -0.2 V_{RHE}.[69]

Single metal atoms can also be anchored in the vacancies of graphene and coordinate with C atoms.[78, 90-91] Ni-C and Ni-N coordination may coexist in N-doped graphene supported Ni single atom catalysts.[78] Characterized by atom probe tomography (ATP) technology, most of the Ni atoms in the NiN-GS catalyst were coordinated with C atoms. Different Ni coordination configurations were proposed (Figure 4c). The calculated free energy diagram at equilibrium potential revealed that the Ni sites trapped in single and double vacancies in graphene with and without N doping were active and selective for CO_2-to-CO.[90]

Apart from N and C coordinated atoms, the single metal atoms can also bond with O[92-94] and S[95] or form metal-metal bonds,[96] resulting in different electronic and geometric properties of the central atoms. In summary, the coordination environment of the single atoms in SACs, including the coordinated atoms, coordination numbers and the second- and high-coordination shell, has a significant effect on the microscopic properties and catalytic performances of SACs.[97] To precisely control the coordination environment of SACs by elaborated synthetic methods and to elucidate the surroundings of SACs by advanced characterization techniques are of great importance to increase the catalytic performance and unveil the structure-activity relationship of SACs.

2.4 Hydrogen evolution reaction (HER) suppression on single-atom sites

Many SACs present excellent CO_2 to CO selectivity, indicating the competing HER is efficiently limited. One of the major advantages of SACs compared to non-SACs is thought to originate from the inherently isolated active sites in SACs. In aqueous electrolyte, the activation of CO_2 on single atomic sites has been experimentally confirmed. Therefore, the competing H_2O adsorption may be suppressed on these isolated sites. In contrast, nanostructured catalysts have continuous surfaces, on which the adsorption of CO_2 and H_2O may occur simultaneously. On the

other hand, as most of those nanostructured metal-based catalysts are polycrystalline, where the different facets often exhibit different binding strengths toward CO_2, H_2O and intermediates.

To elucidate the inhibition of the HER on SACs, DFT calculations were performed. Back et al. compared the free energy change of the initial protonation steps of CO_2RR and HER and found that the formation of *COOH or *OCHO was more favorable than that of *H on most single-atom catalysts (Figure 5a).[91] Similar results have been obtained on Fe-N_4 sites and Ni atomic sites.[64, 78] According to Bagger et al., due to the unique local structure of single atomic sites with a porphyrin-like structure, the HER is forced to proceed via a Volmer-Heyrowsky mechanism, which is less energetically favorable compared with Volmer-Tafel mechanism on metal surface (Figure 5b).[84] On the other hand, the DFT calculations also demonstrated that the *H absorbed on the top of the porphyrin-like sites is weaker than the hollow sites in the metallic catalysts.[84]

The limiting potential, U_L, is another important descriptor that implies the understanding of selectivity of CO_2RR.[79, 98] A more negative calculated $U_L(H_2)$ value for single Ni atom than that for single Co atom or Au(111) indicates an enhanced HER suppression on Ni atomic sites.[78] The difference between thermodynamic limiting potentials ($U_L(CO_2)$-$U_L(H_2)$) reflects the selectivity towards CO_2RR against HER. The larger the value is, the better selectivity towards CO will be achieved.[99-100] For instance, Li et al. proposed the Ni-N_4-C catalyst possessed a larger value of $U_L(CO_2)$-$U_L(H_2)$ than that of N-C (Figure 5d) showed the maximum FE_{CO} of 99%.[85]

Based on the above theoretical calculations, the favorable adsorption of carboxyl (*COOH) or formate (*OCHO) over hydrogen (*H) on SACs provide insight into why many SACs have shown great selectivities for the CO_2RR over the competing HER at low or medium overpotentials. However, because of the poor solubility of CO_2 (~34 mM) and its equilibria in aqueous electrolytes, the diffusion limitation of CO_2 becomes significant at relatively large overpotentials, which also leads to a great challenge to achieve high CO_2RR reaction rates in a conventional H-cell. Most studies focus on the CO_2RR at low or moderate overpotential region, where the effects of CO_2 diffusion are minor and thus the comparison of the catalytic performance of the catalysts is meaningful. To deal with the solubility issue of CO_2 and enhance the kinetics of CO_2RR, different approaches have been developed, such as using flow-cell configurations, lowering the reaction temperature, increasing the pressure for the CO_2RR, or using ionic-liquid based electrolytes.

3 Heterogeneous single-atom catalysts for CO_2RR to CO product

CO is the simplest gas phase product for CO_2RR. According to the progress achieved in this field to date, CO is regard as an economically viable product.[101] Since the 1970s, metal complex molecular catalysts and metal-based electrocatalysts, including Ag, Au and Zn, have been

extensively studied for the CO_2RR to CO.[102-107] In recent years, the heterogeneous SACs have emerged as a promising candidate for the CO_2RR to CO, attracting significant attention. To date, most of these electrocatalysts are fabricated in one of three ways: 1) high temperature pyrolysis of well-mixed metal salts, a carbon source, and a nitrogen source; 2) anchoring transition metal ions on a defective graphene support; 3) Metal organic frameworks (MOFs) derived SACs.

3.1 High-temperature pyrolyzed metal-nitrogen-carbon (M-N-C) catalysts

One facile approach to obtain a heterogeneous catalyst containing atomically dispersed metal sites is to pyrolyze metal precursor with appropriate nitrogen and carbon sources.[108] These materials, usually denoted as M-N-C, have been extensively studied as an alternative for Pt-based catalysts for oxygen reduction reaction (ORR).[109-112]

In 2015, Varela et al. initially explored the use of Fe or/and Mn-containing N-doped porous carbon black heterogeneous catalysts for CO_2RR. The materials were prepared by repeated heat treatments and acid-leaching processes of the well mixed metal (Fe or/and Mn) chloride, polyaniline (PANI) and carbon black precursor powders. X-Ray Diffraction (XRD) combined with transmission electron microscope (TEM) characterization excluded the presence of any metal crystalline phases. They found that the metal free N-C catalyst showed a similar selectivity trend as the M-N-C catalysts while the metal sites led to an enhanced CO_2RR activity and played a key role in the further reduction of adsorbed CO to hydrocarbons as a trace amount of methane also formed at potentials more negative than -0.8 V_{RHE} on Fe-containing catalysts. Based on their experimental observations, they concluded that the nitrogen moieties and the metal sites act as active sites for CO and hydrocarbon production in CO_2RR, respectively. This pioneering work provided a promising alternative M-N-C catalyst for CO_2RR to CO.[47] In the wake of this work, the type of metal in M-N-C catalysts and how these single atom metal sites boost the CO_2RR activity were explored by different groups. Ju et al. explored a series of N coordinated transition metal porous carbon materials (M-N-C, M=Mn, Fe, Co, Ni, Cu) as single site electrocatalysts for CO_2RR. Through an impregnation process of coordinated polymer derived N-doped porous carbons in metal chloride solution and subsequent heat treatments and acid leaching, the M-N-C materials were obtained. The CO_2RR activity test showed that the CO_2RR performance was strongly dependent on the transition metal sites (Figure 6a and b). Fe-N-C reached the maximum FE_{CO} of 65 % at low overpotential of -0.55 V_{RHE}, while Ni-N-C exhibited the highest FE_{CO} of 85 % at -0.78 V_{RHE}. Consequently, Fe- and Ni-N-C catalysts were identified as highly promising catalysts for CO_2RR to CO. The control experiments confirmed that M-N_x sites were the most relevant active centers for CO_2 reduction into CO.[80] Similar trends have been reported by Pan et al. who investigated five transition metals centered M-N-C catalysts for CO_2RR, including Cr, Mn, Fe, Co and Ni, and found

that the CO_2RR performance highly relied on the kind of metal center (Figure 6c and d). They adopted a space-confinement-assisted molecular-level complexing approach to synthesize a series of ultrathin graphene-like M-N-C catalysts. The CO_2RR tests on different transition metal M-N-C catalysts highlighted two superior candidates for CO_2-to-CO, Fe- and Ni-N-C, and identified their different role for promoting CO_2RR. The Fe-N-C catalyst showed a prominently reduced overpotential among all the M-N-C catalysts while Ni-N-C significantly accelerated the reaction rate and enhanced CO selectivity. The highest FE_{CO} of 96 % and the highest TOF of 1060 h^{-1} were achieved on Ni-N-C at a moderate overpotential of 0.64 V.[70]

As the accessibility of single-atom sites and the mass transfer of reactants are crucial for the performance of SACs in heterogeneous catalysis, porous carbon supports with large specific area are favorable for M-N-C catalysts. Hu et al. developed a series of transition metal doped porous carbon materials via silica-templated pyrolysis method.[113] The precursors were prepared by pyrolyzing o-phenylenediamine and metal salts in the presence of silica as template. The catalysts were obtained by subsequent alkali etching, acid washing and a second pyrolysis. The XPS and EXAFS analysis demonstrated the atomically dispersion of metal sites with presumable four N atoms coordination configuration in these materials. The silica template contributed to the CO_2RR activity by improving porosity and the degree of N and metal doping. The Ni-N-C catalyst exhibited the maximum FE_{CO} of 93 % at moderate overpotential of 0.56 V and a much higher CO current density at more negative potentials than Fe and Co doped and metal-free catalysts. Interestingly, the M-N-C catalysts showed a quite different CO_2RR activity trend with the metal porphyrin counterparts, suggesting the metal-nitrogen coordination configuration in pyrolyzed M-N-C may be different from the square planar metal-nitrogen coordination with a D_{4h} symmetry in metal porphyrins.[113-114] Commercially available Fe_2O_3 nanopowder was also used as a template to create pores and increase Fe doping in the Fe,N-doped porous carbon electrocatalysts. It was found that the degree of graphitization of the porous carbon materials plays a key role in CO_2RR.[115]

During the high-temperature pyrolysis process, other metal species (metal nanoparticle or metal carbides) are commonly generated alongside single-atom sites and they cannot be removed even by acid etching in some cases.[110, 116-117] The inhomogeneity of the active sites in pyrolyzed M-N-C catalysts poses a challenge to identify the real active species in CO_2RR. Huan et al. tried to distinguish the crucial structure of Fe active species that determined the selectivity toward CO_2RR and HER. The Fe-N-C catalysts were synthesized by pyrolysis of ZIF-8, ferrous acetate, and 1,10-phenanthroline. The Mössbauer spectra of the catalysts revealed the various Fe species in the catalysts, including several different Fe crystalline structures and atomically dispersed FeN_4 species. The square-planar $Fe^{II}N_4$ or $Fe^{III}N_4$ species are recognized as atomically dispersed Fe in the catalyst. By varying the amount of Fe added and the homogenization method, the relative ratio of FeN_4 to crystalline Fe species can be tuned. Controlled-potential electrolysis in CO_2 saturated 0.5 M $NaHCO_3$ indicated that the catalyst that contained the highest ratio of FeN_4 species (97 %-100 %)

exhibited the highest FE_{CO} of ~80 % at −0.5 V_{RHE}, while catalysts with crystalline Fe as the major Fe species exhibited very high selectivity to H_2 at all tested potentials. The ratio of CO and H_2 as a function of the relative content of FeN_4 sites confirm the key role of FeN_4 moieties for CO_2RR activity.[118]

Apart from metal species, different N species and positively charged C atoms have been considered to be active for CO_2RR.[9, 119-124] The contribution of N species in M-N-C catalysts to CO_2RR should be noted. Nitrogen exists in M-N-C catalysts in different forms, including pyridinic-N, pyrrolic-N, graphitic-N, oxidized-N, and metal-N_x.[47, 125] Nathaniel et al. proposed that both the single atom Fe-N_x sites and the pyridinic N contributed to CO_2RR activity.[126] They added a second nitrogen source during the pyrolysis of aniline, $FeCl_3$, ammonium persulfate and pretreated carbon. After heat treatment, the excess residual Fe species were removed by repeated acid wash and heat treatments. It was found that the choice of the secondary nitrogen source had a significant impact on the Brunauer-Emmett-Teller (BET) surface area, content, and the distribution of nitrogen species. The best CO_2RR performance was achieved on melamine-added Fe-PANI catalyst with a FE_{CO} of 85 % at around −0.6 V_{RHE}. BET surface area normalized CO partial current presented good correlation with the Fe-N species and pyridinic N species contents, suggesting that Fe-N_x and pyridinic N species both contributed to the activity. Pyrrolic N was also reported to function concertedly with Ni-N moieties for CO_2RR to CO.[127] The choice of nitrogen precursor was found to be crucial for achieving high density of active sites and boosting CO_2RR performance. Compared with other nitrogen precursors, polyacrylonitrile (PAN) contributed to higher N content and larger number of Ni-N sites in the pyrolyzed catalysts. The CO_2RR test and controlled experiments revealed that the pyrrolic N and Ni-N sites are the main active components for CO_2RR to CO.

Single metal atoms are mainly coordinated with N atoms forming atomically dispersed M-N_x sites in the pyrolyzed M-N-C catalysts. The coordination number of the metallic atoms significantly influences the properties of the active sites and the catalytic performance of CO_2RR. A Ni-N_4-C catalyst featuring exclusive Ni-N_4 sites was obtained through a topo-chemical transformation strategy.[85] With the help of this strategy, the Ni-N_4 structure was preserved and the formation of Ni particles was prohibited. The EXAFS fitting results showed that Ni coordinated with four N atoms in Ni-N_4-C material. N K-edge XAS combined with N 1s XPS spectra indicated that it is pyridinic-N that bond with single Ni atoms. The Ni-N_4-C catalyst exhibited an unprecedented maximum FE_{CO} of 99 % with a current density of 28.6 mA/cm^2 at −0.81 V_{RHE}. The boosted CO_2RR performance was ascribed to a lowered energy barrier for CO_2 reduction and a faster charge transfer.[85] Molecular electrocatalysts with well-defined M-N4 structure, such as metal porphyrins and metal phthalocyanines, have shown great selectivity towards CO product for CO_2RR.[25-26] Pan et al. increased the M-N coordination number to 5 by anchoring cobalt phthalocyanine (CoPc) on hollow N-doped porous carbon spheres (HNPCSs) and found that pyrolysis temperature had a significant

effect on the coordination environment of Co sites. The strong interaction between Co in CoPc and N in HNPCSs resulted in a Co-N coordination number of 5 in Co-N5/HNPCSs catalyst. The Co-N coordination number decreases to 4 and 3 when Co-N5/HNPCSs was pyrolyzed at 400 and 600 ℃, while Co nanoparticles formed at higher temperatures (800 and 1000 ℃). The FECO decreased with the decrease of Co-N coordination number. The Co-N_5/HNPCSs catalyst exhibited the highest FECO over 99 % at −0.73 to −0.79 VRHE and the highest TOF value of 480.2 h-1 at −0.73 VRHE.[86]

As the atomically dispersed metal sites play a key role in the catalytic performance of SACs, increasing the density of single atom site is a promising way to boost the CO_2RR activity.[128] Although various synthetic approaches have been developed to prepare SACs, fabricating SACs with high loading on carbon-based materials remains a challenging task.[31] Cheng et al. reported a Ni single atoms catalyst supported on N-doped carbon nanotubes (NiSA-N-CNTs) with an ultrahigh Ni loading up to ~20 wt.% and outstanding CO_2RR activity.[129] The catalysts were synthesized by a facile multistep pyrolysis method with a well-mixed precursor of dicyandiamide and nickel (II) acetylacetonate. In the multiple pyrolysis stages, the Ni-O-C structure, Ni-doped g-C_3N_4 and atomically dispersed Ni atoms with Ni-N_4 structures were formed in sequence. The Ni content in NiSA-N-CNTs catalyst, as determined by X-ray energy-dispersive spectroscopy (EDS), was 19±3 wt.%. The linear combination analysis of Ni L-edge XANES spectra revealed that about 88±2% of Ni atoms are in the form of Ni-N. The maximum FE_{CO} of 91.3 % with a CO partial current of 23.5 mA/cm^2 was achieved on the NiSA-N-CNTs catalyst at −0.7 V_{RHE}. According to the change of the XANES spectra of Ni K-edge and N K-edge before and after electrolysis, the Ni-N species was inferred to be the active center for CO_2RR to CO.[129] They also systematically investigated the formation mechanism of the NiSA-N-CNT catalysts and the effect of their preparation conditions on the CO_2RR performances. The transformation from stacked Ni-g-C_3N_4 layer to bamboo-like tubular NiSA-N-CNT catalyst was conjectured to undergo a rolling-up process, in which the mobile Ni single atoms played a vital role. The optimal Ni(acac)$_2$:DCD ratio and annealing temperature were 1:200 and 800 ℃, respectively.[130] Although the single atom density was greatly enhanced in these works, the CO_2RR activity was not improved as much as the metal loading. It should be noted that not all the metal atoms were in the form of active single-atom sites. On the other hand, part of the single atomic sites may locate in the walls of carbon nanotube and become inaccessible.[117]

As discussed above, Ni-based single atom catalysts are an outstanding candidate for CO_2RR to CO.[75, 80, 113] The unique electronic and geometry structure and the structural transitions in CO_2RR of the single Ni atomic sites were crucial to understand the origin of the high CO_2RR performance of single-Ni-atom catalyst, which was discussed by Yang and co-workers.[75] The catalysts prepared by pyrolyzing nickel acetate and melamine with L-alanine and L-cysteine (sulfur-containing amino acid) were denoted as A-Ni-NG and A-Ni-NSG. The single Ni atoms featured monovalent with unpaired electron in 3d orbital and were identified as the active site in both catalysts. Geometrically, the highly distorted symmetry around the Ni atoms in A-Ni-NSG catalysts could also promote the

adsorption of reactants and intermediates. Consequently, the unique electronic and geometric structure guaranteed the great catalytic performance of A-Ni-NSG catalyst. Characterized by XPS and operando XANES and EXAFS spectra, the CO_2 activation by the charge transfer from the 3d orbital of monovalent Ni atomic site to 2p orbital in CO_2 was observed in CO_2-saturated electrolyte. During the CO_2RR at -0.7 V_{RHE}, the active Ni site recovered to low-oxidation state after a CO_2 reduction cycle.

In traditional H-type electrolyzer, the current density is limited by the low solubility of CO_2 (34 mM at standard conditions) in aqueous electrolyte, which hinders the commercial application of CO_2RR. By the facile pyrolysis strategy. Ni-based SACs have been fabricated at gram-scale and their CO current density were dramatically increased using improved electrode and reactor designs. Zheng et al. synthesized a Ni SACs (Ni-NCB) at gram-scale via a simple and scalable approach (Figure 7a). The CO_2RR tested in a H-cell demonstrated that the optimized Ni-NCB catalysts exhibited a high FE_{CO} over 95 % in a potential range from -0.6 to -0.84 V_{RHE} and an impressive stability during a 24 h continuous CO_2-to-CO electrolysis, which is due to the stable Ni atomic sites in the catalyst. When an anion membrane electrode assembly (MEA) was employed, the Ni-NCB catalyst exhibited nearly 100 % FE_{CO} at high current density up to 130 mA/cm^2. Further scaling up the anion MEA size to 10*10 cm^2 (Figure 7b), a record high current density of 8.3 A and a CO generation rate of 3.42 L/h were achieved at a full-cell voltage of 2.8 V. [131] Tim et al. carried out CO_2RR in a micro flow cell electrolyzer and reached an industrial current density up to 700 mA/cm^2. They synthesized the Ni and Fe based nitrogen-doped porous carbon catalysts (Ni- and Fe-N-C) using a similar method reported by their group.[126] In addition to the Ni-N_x moieties, the Ni-N-C catalyst contained some crystalline Ni species as confirmed by XRD and TEM, which were acid-insoluble, densely encapsulated and unlikely to participate in the CO_2RR. The Ni-N-C catalyst was deposited on a gas diffusion electrode to integrated with a flow cell electrolyzer (Figure 7c). Between the current densities of 100 and 200 mA/cm^2, the Ni-N-C catalyst exhibited a FE_{CO} of nearly 90 %, outperforming N-C, Fe-N-C, and AgO_x benchmark catalysts (Figure 7d and e). The result demonstrated the great potential of the Ni-N-C catalyst for CO_2RR at high current density.[132]

Although Fe and Ni doped M-N-C catalysts are frequently studied as electrocatalysts for CO_2RR, other atomically dispersed metals have also been demonstrated to be active for CO_2RR to CO with high FE. Zinc is a CO-producing metal for CO_2RR. Various nanostructured Zn catalysts have been constructed to convert CO_2 to CO, such as porous Zn catalysts,[133-134] Zn nanoparticles,[135] Zn nanosheet,[136] and Zn dendrites[137]. Similar to its metal/oxide counterparts, single atom Zn catalysts have also been reported to convert CO_2 into CO through CO_2RR. By high temperature pyrolysis and acid leaching process, Zn coordinated N co-doped graphene catalyst (Zn-N-G) was prepared and presented high activity and selectivity to CO during CO2RR. The Zn-N-G catalysts retained the morphology of graphene sheets. XPS and EXAFS spectra confirmed

that the single Zn sites coordinated with N to form Zn-N_x moieties with a coordination number of 3.6 ±0.5. The maximum FE of CO reached 90.8 % at a low overpotential of 0.39 V (-0.5 V_{RHE}) and a high CO current density of 11.2 mA/cm^2 was achieved at -0.8 V_{RHE}. The Zn-N_x sites were deemed to be the main active centers for CO_2RR to CO.[138] Similarly, Yang et al. reported a carbon supported nitrogen-anchored Zn single atom catalyst (ZnN_x/C) prepared by pyrolyzing a mixture of carbon black, urea and zinc acetate. The optimal catalyst achieved a maximum FE_{CO} of 95 % at -0.43 V_{RHE} and maintained a steady current density at ~ -4.8 mA/cm^2 at this potential during a 75 h long-term stability test. Density functional theory (DFT) calculation showed that the free energy barrier for the rate determining step of *COOH formation was significantly lower on Zn-N_4 sites than on N-C or Zn-C sites, confirming the atomically dispersed Zn in the form of Zn-N_4 was the active sites for CO_2RR.[139] Owning to the relative low melting point (692 K) and boiling point (1180 K), Zn tends to lost through evaporation under high temperature pyrolysis.[140-142] Considering that increasing the metal loading is believed to be a promising way to improve the activity of SACs, atomically dispersed Zn-N-C catalyst with high Zn loading is favorable.[12, 128] Tin (Sn), together with a few main group metals like Pb, Bi and In, mainly produce formate in aqueous solution.[143-144] Various nanostructured Sn-based catalysts have been extensively studied for its good selectivity to formate, low-cost, and eco-friendly nature.[145-154] Downsizing the dimension of Sn-based catalysts has been proved to be favorable to high CO_2RR activity.[155-156] Further, reducing the size of Sn-based catalysts to single atomic scale has not been reported until recently. Zhao et al. developed a N-doped porous carbon nanofiber supported Sn catalyst for CO_2RR. The fibrous catalyst was prepared by an electrospinning technique and a subsequent pyrolysis process. Sn nanoparticles decorated onto a N-doped carbon catalyst exhibited similar catalytic selectivity to Sn metal or Sn oxide catalysts with formate as the main product. However, the atomically dispersed Sn on N-doped carbon nanofibers obtained by leaching out Sn particles showed a high selectivity toward CO (FE_{CO} of 91 % at -0.6 V_{RHE}). The XPS spectra revealed that the valence of atomically dispersed Sn was between 0 and +2, which may be stemmed from the formation of Sn-N moiety. The enhanced CO_2RR performance was mainly attributed to the enhanced stabilization of $CO_2^{\cdot-}$ and facilitated formation of COOH* intermediates on single Sn atomic sites.[157] Antimony (Sb) is a main group metal that resides alongside Pb, Sn and Bi on the periodic table of elements and is barely used as electrocatalysts for CO_2RR. Jia et al. prepared N-doped carbon supported Sb SACs that displayed efficient CO_2RR activity. The Sb SACs was prepared by pyrolysis of mixed $SbCl_3$, urea and active carbon black. The Sb SACs exhibited the maximum FE_{CO} of 82 % with a CO current density of 2.4 mA/cm^2 at -0.9 V_{RHE}. By selectively blocking the pyridinic N sites by H_3PO_4, the FE and current density of CO decreased, indicating the pyridinic N sites also promoted CO_2RR.[158]

The high-temperature pyrolyzed M-N-C catalysts, which have been widely studied as promising non-precious metal ORR catalysts, have shown their great potential in CO_2RR. The high

activity and selectivity, low-cost, and facile preparation methods of the M-N-C catalysts underlies their practical application for CO_2RR. However, some obstacles are still needed to be deal with: 1) the formation of the single atomic sites remains elusive; 2) to control the homogeneity of the active species during the pyrolysis process is challenging while promising to elucidate the structure-performance relationship; 3) the decisive property of the center metal atoms of SACs for CO_2RR is unclear as a variety of center metals, including the major Ni and Fe, as well as Zn, Sn, and Sb are active for CO_2RR to CO; 4) the influence of the pyrolysis conditions on the structure of the catalyst and the catalytic performance need to be clarified.

3.2 Graphene supported SACs for CO_2RR

Graphene offers a great platform for loading single atoms due to its two-dimension (2D) structure, high specific area, high electrical and thermal conductivity, and abundant surface functional groups and defects. Apart from binding with N atoms in N-doped graphene, the strong binding of single metal atoms with the single- and double-vacancies on graphene also guaranteed the structural stability of catalysts.[91] Although thermal treatment is usually involved in fabricating graphene supported SACs, taking advantage of graphene instead of organic carbon precursors or carbon black endows the SACs with unique coordination structure, great conductivity, a large specific surface area, and improved accessibility of single atomic sites. Therefore, graphene supported single-atom electrocatalysts for CO_2RR have been drawing great attention in recent years.

In 2016, Su et al. prepared a Ni and N modified graphene as an electrocatalyst (Ni-N-Gr) for CO_2RR. To avoid the breakage of Ni-N bond under high temperature, they treated the precursor containing Ni pentaethylenehexamine and graphene oxide at 900 ° C in Ar atmosphere for 45 seconds and then leached the sample by acid. Single Ni atoms coordinated with N atoms was confirmed by XPS and EXAFS results. The Ni-N-Gr catalyst exhibited a high FE_{CO} over 90 % within potential of -0.7 to -0.9 V_{RHE}. The high CO_2RR activity was attributed to the atomic Ni coordinated with N sites on the graphene. Similar TOF values were obtained on two Ni-N-Gr catalysts with different amount of Ni, suggesting the intrinsic CO_2-to-CO activity of the Ni-N active center.[159]

The introduction of nitrogen in the graphene is important for the formation of graphene supported SACs. Zhang et al. annealed the lyophilized mixture of graphene oxide and $FeCl_3$ in NH_3/Ar atmosphere to introduce nitrogen. The nitrogen was believed to anchor Fe atoms through metal-nitrogen coordination.[63] The Fe species mainly existed in the form of single Fe atoms in the Fe/NG-750 catalyst annealed at 750 °C, which exhibited a maximum FE_{CO} of ~80 % at -0.6 V_{RHE}. However, metallic Fe and Fe_3O_4 nanoparticles formed at higher temperature (800 ℃) or with the

excess amount of $FeCl_3$, exhibited poor FE_{CO} less than 10%. Combined the XAFS result and CO_2RR performance, they concluded that the atomically dispersed pyridinic Fe-N_4 sites was largely responsible for the enhanced CO_2RR activity. Furthermore, Fe-free and no N-doped catalysts both presented poor CO_2RR activity, substantiating the synergistic effect between N and atomically dispersed Fe species on graphene for CO_2RR activity. [63]

The N doping could also change the morphology and coordination environment of graphene supported SACs, resulting in the disappearance of small metallic clusters that existed in the catalyst annealed in H_2/Ar atmosphere.[78] Jiang et al. prepared a graphene layer supported single atom Ni catalyst (Ni-NG) for CO_2RR to CO by annealing freeze-dried Ni^{2+}/GO powder at 750 ℃ under NH_3/Ar atmosphere. The presence of Ni nanoparticles and clusters was excluded by TEM and the single Ni atoms were observed by aberration-corrected HAADF-STEM. The Ni-NG catalysts exhibited a maximum FE_{CO} of ~95 % with a current density of ~11 mA/cm^2 at an overpotential of 620 mV and a stable CO_2RR performance for more than 20 h. The control experiments highlighted the importance of N doping for boosting CO_2RR to CO activity and selectivity. Furthermore, the obvious differences of XANES and EXAFS spectra between Ni-NG and Ni porphyrin revealed that the single Ni atoms were not only coordinated with N atoms. Instead, single Ni atoms embedded in vacancies in graphene was brought up, such as single Ni atom fitted in single vacancies and double vacancies in graphene.[78] It's worth noting that N coordinated metal sites were suggested to be the main active center for the CO_2RR on pyrolyzed M-N-C catalysts. However, graphene with abundant defects and vacancies provides anchoring sites for metal atoms, which led to unique structure and coordination of the single atoms. By three-dimensional atom probe tomography (APT) technology, that single Ni atoms in graphene vacancies were directly evidenced. The carbonized Ni and N containing polymer nanofiber (NiN-GS) showed uniformly dispersed Ni nanoparticles encapsulated by graphene shells and isolated Ni atoms incorporated in the graphene shell. The NiN-GS catalyst deposited on a glassy carbon electrode presented the highest FE_{CO} of 93.2 % at an overpotential of 0.7 V with a CO partial current density of ~4 mA/cm^2. The Ni atoms in the graphene shell was identified as the major factor for the improved CO_2RR performance. To elucidate the state of the Ni atomic sites, three-dimensional APT technology was applied. The statistical analysis of single Ni atoms dispersed area indicated that 83 % of Ni atoms were in single atom form, while most of the single Ni atoms were coordinated with C atoms and only 0.2 % of them were coordinated with one N atom. However, these N atoms were found to be vital for the generation of defects in the graphene shell which helped to trap Ni atoms.[90]

N-doped graphene could also provide an axial N ligand, by which a novel Fe-N_5 site could be achieved by anchoring Fe-N_4 sites with N ligand from the N-doped graphene.[160] Zhang et al. used melamine to crosslink with ferric chloride heme and introduced N sites into graphene during the high-temperature pyrolysis. The structure of FeN_5 sites formed by axial coordination between FeN_4

and N-doped graphene were verified by performing XANES spectra analysis and DFT calculation. The FeN_5 catalysts started to catalyze CO_2 to CO at an overpotential of 0.15 V and reached the maximum FE_{CO} of 97.0 % at −0.46 V_{RHE}. Although FeN_4 possessed a higher content of Fe and N than FeN_5, it exhibited an inferior CO_2RR performance to FeN_5. The additional axial N ligand in FeN_5 withdrew the d electron from Fe and resulted in a higher oxidation state of Fe atom, which reduced the Fe-CO π back-donation and facilitated the CO desorption.[160]

A highly porous carbon matrix with high density of surface defect sites is desired to achieve efficient SACs for CO_2RR. The former maximizes the formation of $M-N_x$ sites while the later facilitates the accessibility and utilization of these sites. In this regard, Cheng et al. developed a Ni single atom catalyst on microwave exfoliated graphene oxide (Ni-N-MEGO) featuring high Ni loading (~6.9 %) and large surface area (2380 m^2/g). The aberration corrected STEM images showed that the Ni atoms are predominately anchored on the edge of the pores, exposed basal-plane edges and steps of graphene sheets. X-ray absorption spectroscopy indicated that Ni atoms mainly coordinated with N in both unsaturated $Ni-N_2$, $Ni-N_3$ and well-defined $Ni-N_4$ moieties in the catalyst. DFT calculation results demonstrated that these edge-anchored unsaturated Ni sites exhibited favorable energy for CO_2 activation and CO desorption than the in-plane sites. Consistent with the simulation, a low onset overpotential of 0.18 V, high FE_{CO} of 92.1 % and a large CO current density of 26.8 mA/cm^2 (at −0.7 V_{RHE}) were obtained on Ni-N-MEGO in CO_2-saturated 0.5 M $KHCO_3$ solution. The high loading of unsaturated Ni single atoms on edges was believed to account for the high CO_2RR activity.[117]

In summary, the advantages of employment of graphene supported single-atoms catalysts for CO_2RR can be mainly described as: 1) ultrathin 2D structure and abundant surface defectives enrich the surface single-atom sites; 2) large specific surface area facilitates the utilization of single-atom sites; 3) excellent conductivity promotes the electron transfer. Furthermore, the specific graphene vacancies (single and double vacancies) could accommodate isolated metal atoms, forming unique coordination environment.[78] The introduction of nitrogen by either addition of nitrogen sources or annealing in ammonia atmosphere is crucial for the graphene supported SACs. The ‘electrocatalysts prepared without N showed poor CO_2RR activity.[63, 78] However, the critical role of N dopant is not conclusive and needs further investigation.

3.3 MOF derived SACs for CO_2RR

Metal-organic frameworks (MOFs) as a class of coordination polymers featuring open frameworks, high specific surface area, and abundant metal ions coordinated with diverse organic ligands.[161] Some MOFs show outstanding CO_2 adsorption capacity,[162] which is prerequisite for

reduction of CO_2. Thus, MOFs with different metal nodes are promising and have been studied as catalysts for CO_2RR.[163-165] Recently, converting the organic ligands of MOFs into N-doped carbon materials by heat treatment not only maintains the merits of MOFs but also improves the electrical conductivity of the catalysts.[166-167] Either metal-containing nodes/linkers or absorbed metal ions in MOFs can turn into atomically dispersed M-N_x sites during the heat treatment.[168] The preparation of MOFs-derived SACs for CO_2RR usually involves pre-introduction and post-modification strategies to prevent the aggregation of the metal atoms.

The former strategy involves the incorporation of target metal salts during the crystallization of MOFs and the subsequent pyrolysis process to form the isolated metal atoms in the carbon matrix. There are two ways to introduce the target metal atoms, 1) incorporating the target metal atoms as either metal nodes or metal-coordinated linker into the framework of MOFs, 2) spatial confining the target metal precursors inside the cages and pores of MOFs.[169-172] During the subsequent pyrolysis process, the MOFs were converted into N-doped carbon materials and the incorporated metal precursors form atomically dispersed sites.

Zn-based zeolitic imidazolate frameworks (ZIF-8), which is consisted of Zn cations as metal nodes and imidazolate as organic linkers, is an ideal substrate to fabricate MOFs-derived SACs for CO_2RR. Zn has a relative low boiling point (907 °C) which can easily evaporate during the pyrolysis and create a highly porous structure and leave anchoring sites for target metal atoms while imidazolate organic ligands can be carbonized to a porous N-doped carbon support. Pan et al. introduced Fe or Co ions during the growth of ZIF-8 and Fe and Co ions substituted some Zn^{2+} ions to chemically bond with 2-methylimidazole, thus ensuring the uniform distribution of Fe and Co in the precursor. In the subsequent heat treatment, atomically dispersed Fe or Co sites coordinated with four N atoms were formed in the carbon matrix. The CO_2RR test manifested that Fe-N-C catalyst exhibited a better CO_2RR performance than Co-N-C and metal-free N-doped carbon catalysts. The DFT calculation revealed edge-hosted Fe-N_4 moiety where two N-doped graphitic layers are connected by a Fe atom through two N atoms in each layer, is thermodynamically and kinetically active for the CO_2RR.[51] Given the competing HER seems to be inevitable under the CO_2RR conditions and the syngas product with a suitable CO/H_2 ratio is also desirable, Song et al. constructed a single Co atom catalyst by annealing process of ZnO@ZIF heterostructure to produce syngas via CO_2RR. The reduced Zn evaporated, resulting the formation of hollow and porous structure and promoting the formation of single Co atoms. The EXAFS fitting results showed that about 84.7 % of Co was existed as single atom in the form of planar Co-N_2C_2. The CO selectivity was found to be proportionate to the ratio of Co-N_x/(pyridinic N+graphitic N+Co-N_x) in Co-HNC catalyst. Accordingly, the authors proposed a dual-site mechanism in which atomic Co-N_2C_2 sites act as CO_2RR active center while N functional group as HER active center, which was further confirmed by potassium thiocyanate (KSCN) poisoning experiments and DFT simulations.[173]

The coordination structure of metal atom in MOFs-derived SACs could be modulated by the heat treatment process of the precursor MOFs. Geng et al. tried to regulate the coordination environment of single Co atom catalysts by varying the temperature of heat treatment and explored its effect on CO_2RR performance. The Co species existed in single-atom form in the catalysts of Co_1-N_4 and Co_1-$N_{4-x}C_x$, which were prepared by pyrolyzing a ZnCo bimetallic MOF at 800 °C and 900 °C, respectively. According to the XAFS analysis, especially the wavelet transform of Co K-edge, the authors speculated that part of Co-N coordination was replaced by Co-C at elevated temperatures for Co_1-$N_{4-x}C_x$ while the total coordination number of the first shell of Co atom remained 4. The CO_2RR test demonstrated that Co_1-N_4 catalyst exhibited a better performance than Co_1-$N_{4-x}C_x$ at all tested potentials. The comparable charge transfer resistance and electrochemical surface areas of these two catalysts implied the different intrinsic active of the Co active sites in the catalysts. The enhanced CO_2 binding strength and CO_2 adsorption capacity of Co_1-N_4 catalyst was believed to be the main reason for the enhancement CO_2RR performance.[88] However, different result was reported by Wang et al. who found that single Co atom catalysts with lower Co-N coordination number exhibited better CO_2RR performance. Three catalysts, Co-N_4, Co-N_3 and Co-N_2, were prepared by pyrolyzing ZnCo bimetallic ZIFs at 800, 900 and 1000 ℃, respectively. The fitting results for EXAFS data revealed that the Co-N coordination number decrease gradually from 4.1 to 2.2 with the elevated temperature in these three catalysts. Meanwhile, a decreased oxidation state of Co was observed with the decreased Co-N coordination number. The CO_2RR test demonstrated that the Co-N_4 catalyst exhibited negligible activity and poor CO selectivity, while the Co-N_2 catalyst reached the highest FE_{CO} of 95% at -0.68 V_{RHE} and a high TOF of 33000 h^{-1} at -0.78 V_{RHE}. Further, the authors intentionally increased the Co-N coordination number from 2 to 4 by NH_3 treatment of Co-N_2 at 400 ℃ and the NH_3-treated Co-N_2 catalyst exhibited a significantly decreased CO_2-to-CO activity. Based on the DFT calculation results, the reduced energy barrier for the formation of $*CO_2^{\bullet-}$ on Co-N_2 sites explains its high CO_2-to-CO activity while high energy are needed for the formation of both $*CO_2^{\bullet-}$ and *H on Co-N_4.[65]

Single Ni atom catalysts can also be prepared by pyrolyzing Ni doped bimetallic ZIF-8 at high temperature (Figure 8a) and the Ni loading reached as high as 5.44 wt.% in carbonized C-Zn_1Ni_4 ZIF-8 sample.[87] The catalyst exhibited high FE_{CO} over 92% in a wide potential range of -0.53 to -1.03 V_{RHE} and a high CO current density of 71.5±2.9 mA/cm^2 at -1.03 V_{RHE}. The fitting results of EXAFS data revealed that the Ni atoms were coordinatively unsaturated. It should be noted that Zn atomic sites also existed in the samples, even though Zn tends to evaporate at high temperature due to their low boiling point.[65, 174] The CO current density increased with the Ni content but decreased with Zn content, indicating the coordinatively unsaturated Ni-N_x sites were the active sites for

CO_2RR. The DFT simulation demonstrated that the free energy of *COOH was lower on the coordinatively unsaturated Ni sites than that on Ni-N_4 sites.[87]

It is well-known that N atoms exist in different forms in N-doped carbon materials. The different kinds of N ligand also influence the coordinated center metal atoms, leading to different catalytic performance. For instance, Fe-pyrrolic N moieties in single-atom iron catalysts was regarded as the origin of high oxygen reduction reaction activity.[175] For CO_2RR, pyridinic nitrogen coordinated M-Nx sites are usually regarded as the active centers of SACs. Recently, Gu et al. reported a Fe^{3+}-N-C catalyst with discrete Fe^{3+} coordinated to pyrrolic-N atoms in a N-doped carbon support by pyrolyzing Fe doped ZIF-8. The oxidation state of Fe in Fe^{3+}-N-C catalyst was determined to be +3 from the Fe $2p_{3/2}$ XPS spectrum and the Fe K-edge XANES spectrum. The CO_2RR experiment on Fe^{3+}-N-C catalyst in an H-type cell showed that CO was detected at as low as -0.19 V_{RHE} (overpotential of 80 mV) and a high CO partial current density of 20 mA/cm^2 was achieved at -0.47 V_{RHE}. A critical applied potential of -0.5 V_{RHE} was observed, below which the CO_2RR activity of Fe^{3+}-N-C catalyst decreased obviously. By operando XAS characterization, the coincidence of the change in activity and oxidation state revealed that Fe^{3+} sites are more active than Fe^{2+} for CO production. Compared with Fe^{2+} sites, the faster CO_2 adsorption and the weaker CO binding of Fe^{3+} sites were responsible for the better catalytic performance. The pyrrolic N ligands were speculated to play a key role in improving the stability of Fe^{3+} state under reaction condition, thereby high activity could be maintained.[69]

The single atomic sites can also be obtained through the post-modifications of MOFs, namely introducing the target metal atoms after the crystallization of MOFs. Zhao et al. adopted a double-solvent approach to confined Ni ions in the pores of the pre-synthesized ZIF-8 (Figure 8b). In the subsequent pyrolysis process at 1000 ℃, the organic linkers converted to N-doped carbon material and Zn evaporated. The N-rich defects generated by Zn evaporation stabilized the Ni^{2+} ions to form single Ni atom sites coordinated with three N atoms in the Ni SAs/N-C catalyst. The Ni SAs/N-C catalyst reached the maximum FE_{CO} of 71.9 % at -0.9 V_{RHE} and a CO current density of 7.37 mA/cm^2 at -1.0 V_{RHE}. The fast electron transfer determined by Nyquist plot for Ni SAs/N-C catalyst promoted the formation of $CO_2^{\bullet-}$ radical anion and the low-coordinated single Ni sites bonded strongly with the $CO_2^{\bullet-}$ and facilitated its further reduction.[174]

Exposure and accessibility of active sites of the catalysts cannot be neglected for heterogeneous catalysis. Incorporating metal into MOF by pre-introduction strategy undoubtably buries some of the metal sites deep inside the MOF framework. Anchoring single atomic sites on the surface of the MOFs by post-modification strategy could enhance the utilization of the single atoms. Ye et al. utilized ammonium ferric citrate as Fe source to modify the surface of ZIF-8 through ligand

exchange (C-AFC©ZIF-8). The citrate ion strongly coordinated with Zn^{2+} on the surface of ZIF-8, but cannot penetrate the small pores of ZIF-8 due to its large steric size (Figure 8c). As a contrast, a control sample (C-AFC@ZIF-8) was also prepared by incorporating ammonium ferric citrate during the crystallization of ZIF-8. Although, atomically dispersed Fe atoms with Fe-N bond were formed in both samples with similar Fe content, the C-AFC©ZIF-8 exhibited higher maximum FE_{CO} and larger CO partial current density than C-AFC@ZIF-8, highlighting the importance of the surface single atom sites.[176]

Due to the more strong metal-nitrogen interaction, metal nanoparticles decorated ZIF-8 derived N-doped carbon can be converted to stable SACs (Pd, Pt, Au) at high temperatures in an inert atmosphere.[177] Yang et al. loaded Ni nanoparticles (Ni NPs) on the surface of ZIF-8 derived N-doped carbon and in-situ converted Ni NPs into thermally stable Ni single atom catalyst by a thermal atomization method (Figure 8d).[89] The surface N-rich defects could bond with Ni NPs and were important for the transformation from Ni NPs to Ni single atoms, resulting in porous structure and abundant surface active single Ni atoms. When the Ni NPs diffused on the surface of the N-doped carbon substrate, the Ni atoms were captured by N defect forming surface-enriched single Ni atoms. Due to the porous structure and abundant surface single Ni sites, the catalyst exhibited a high FE_{CO} over 90 % at potential ranging from -0.6 to -1.0 V_{RHE} and a TOF as high as 48842 h^{-1} at -1.1 V_{RHE}.[89] Similarly, a Bi-MOF precursor was converted into single-atom Bi sites on porous carbon by the atomization strategy.[100] Bismuth (Bi) based catalyst is another promising electrocatalyst that can convert CO_2 to formate with a high Faradaic efficiency.[178-179] In this work, the authors demonstrated that atomically dispersed Bi electrocatalysts efficiently converted CO_2 to CO. During the pyrolysis of Bi-MOF, the Bi nanoparticles formed first and then underwent a atomization process with the help of ammonia (NH_3) released from the decomposition of dicyandiamide. The Bi atoms coordinated with four N atoms and exhibited a valence between 0 and +3 in the Bi SAs/NC catalyst. The evaporation of Bi NPs resulted in a high surface area and an abundant pore structure which is beneficial for the accessibility of single-atom Bi sites and mass transfer. The Bi SAs/NC catalysts achieved a maximum FE_{CO} of 97 % with a CO current density of 3.9 mA/cm^2 at -0.5 V_{RHE}. The intentional poisoning test of Bi-N_4 sites by thiocyanate (SCN^-) demonstrated that Bi-N_4 sites are the active for CO_2RR.[100]

The pre-introduction and post-modification of MOFs could be combined to further increase the CO_2RR performance. Recently, Ren et al. developed an atomically dispersed Ni-Fe dual-site catalyst (Ni/Fe-N-C) by combining the two strategies for CO_2RR. The Fe doped ZIF-8 was prepared first and a dual-solvent approach was then used to confine a Ni precursor within the Fe doped ZIF-8. The Ni/Fe-N-C catalyst was finally obtained by a heat treatment at 1000 ℃. The single atoms and many neighboring dual-atoms were observed in aberration corrected HAADF-STEM images. Based on the Ni K-edge XANES and fitting results of EXAFS spectra, a dual-sites model with neighboring Ni-Fe site was proposed. The Ni/Fe-N-C exhibited the maximum

FE_{CO} of 98 % at −0.7 V_{RHE}. The calculated TOF value of Ni/Fe-N-C was 7682 h^{-1}, which was much higher than that of Ni-N-C and Fe-N-C, indicating the higher intrinsic activity of Ni/Fe-N-C. The Ni-Fe dual-sites accelerated the rate of the first electron transfer step and enhanced the kinetics of this rate-determining step for CO_2RR. Based on the DFT simulations, the authors proposed a mechanism for dual-site catalyst where the CO-adsorbed Ni-Fe dual sites show enhanced *COOH binding strength and weakened *CO binding strength, which are beneficial for the CO production. Thereby, on these CO-adsorbed Ni-Fe dual sites, the theoretical overpotential for CO production reduced from 0.76 to 0.47 V.[79]

It can be clearly seen from the above discussion that ZIF-8 is frequently used as the precursor for the MOFs-derived SACs for CO_2RR. Several reasons may account for the choice of ZIF-8: 1) the controllable morphology and well-defined porous structure; 2) the convenient incorporation or modification of ZIF-8 assist the formation of atomically dispersed target metal atoms; 3) the readily evaporated Zn create pores and vacancies; 4) the high content of heteroatoms (N atoms) in the carbonized carbon framework. In the future, more MOFs or COFs derived SACs should be developed to fully harness the advantages of these materials.

4 Challenges and perspectives of SACs for CO_2RR

To date, although SACs have exhibited great promise for CO product, the research on SACs for CO_2RR is still in its infancy. To date, pyrolyzed M-N-C catalysts, graphene supported SACs, and MOFs derived SACs account for the most cases of reported heterogeneous SACs for CO_2RR. The comparison of these methods are summarized in **Figure 9** and the following challenges should be considered in future to advance the development of this field.

4.1 Products beyond CO from SACs

Within the published literature, CO has been shown to be the major product from the CO_2RR on SACs. There may be three main reasons for this phenomenon. 1). Favorable CO production. Based on the theoretical calculations, the single metal sites have an appropriate binding strength for the intermediates, such as *COOH and *CO.[63, 91] Therefore, the formation of *COOH and *CO, as well as the desorption of *CO have moderate energy barriers, which are conducive to the production of CO. 2). The suppressed HER. The activation of CO_2 molecules on single Ni sites in the aqueous solution was observed by operando X-ray absorption spectroscopy and photoelectron spectroscopy.[75] The competing adsorption of *H species may be blocked on these single sites. Furthermore, based on theoretical calculations, the relatively negative limiting potential for H_2

production on SACs implies an inherent HER suppression on these single atom sites.[78] 3). The blocked C_{2+} production. The C–C coupling may be largely blocked as the active sites in SACs are atomically isolated, leading to physical separation of reactive intermediates and subsequent suppression of any C_{2+} product formation.[180] There are at least 16 different products that have been identified in CO_2RR regardless of the significantly different selectivity, yet CO is the dominating reduction product on SACs (Figure 10**Error! Reference source not found.**).[180] Products from CO_2RR beyond CO are more desirable due to their higher energy density. For now, formic acid, methane, methanol and even ethanol have been produced through CO_2RR on heterogeneous SACs.

Formate (including formic acid) is an intriguing liquid production of CO_2 electrocatalytic reduction due to its broad interest in energy storage and conversion. Zu et al. fabricated single Sn atom on N-doped graphene catalyst at kilogram-scale by a quick freeze-vacuum drying-calcination method. The single Sn atom catalyst exhibited an ultralow onset overpotential of 60 mV for formate formation, a maximum FE_{HCOOH} of 74.3 % at −1.6 V_{SCE} (calculated as −0.946 V_{RHE} at the reported pH of 7.1) and a record high TOF of 11930 h^{-1} for CO_2RR to formate (**Figure 11**a). The strong interaction between isolated Sn atoms and neighboring atoms caused the charge density in metal atoms move toward neighboring atoms, resulting in positively charged Sn species on N-doped graphene. The positively charged Sn atoms favored the stabilization of $*CO_2^{\bullet-}$ and $*HCOO^-$ intermediates, thus enabling the CO_2 activation and protonation of $*CO_2^{\bullet-}$ to proceed spontaneously. In addition, the strong N–Sn bond favored the desorption of $*HCOO^-$, leading to the high selectivity to formate.[76] Based on the in situ FTIR analysis, a mechanism of CO_2 electroreduction to $HCOO^-$ via the adsorbed $*CO_2^{\bullet-}$ and $*HCOO^-$ intermediates was proposed on single atom Sn catalyst. DFT calculations revealed that the formation of both $*CO_2^{\bullet-}$ and $*HCOO^-$ intermediates were downhill on the single-atom $Sn^{\delta+}$ on N-doped graphene/graphene due to the electron delocalization on the single Sn atom sites. Consequently, the $*HCOO^-$ desorption became the RDS as single-atom $Sn^{\delta+}$ on N-doped graphene (Figure 11b).[76] Mo-based catalysts are usually considered to be the promising candidates for the competing HER, however, single atom Mo catalysts have also been investigated for CO_2RR. Huang et al. prepared single Mo atom embedded in N-doped graphene and found that the FE of CO_2RR into formate and the production rate of formate on N-doped graphene were greatly boosted by the loaded single Mo atoms. Despite the high overpotential and the relatively low FE, the catalyst presented a high formate production rate of 747 $mmol/(g_{cat}\bullet h)$ for CO_2RR into formate.[181]

Copper based materials are a unique class of CO_2RR catalysts known for its ability to produce deep reduction products, like hydrocarbons and alcohols. It has a moderate adsorption energy for the important intermediates of CO and COOH, resulting poor selectivity of Cu-based CO_2RR

catalysts.[23, 81, 182–186] The CO_2RR to CH_4 undergoes an 8e transfer process. For single atom, especially Fe containing catalysts, trace amount of CH_4 are commonly produced at relative large overpotential accompanied with the major product of CO.[47, 63, 118] Strong CO binding strength between metal sites and CO is required to the formation of CH_4.[47, 80] Wang et al. reported a Cu doped CeO_2 catalysts that reached a high $FE_{methane}$ of ~58 % at −1.8 V_{RHE}. The Cu doped CeO_2 catalyst was synthesized by a wet impregnation method and annealed in a H_2/Ar atmosphere to generate oxygen vacancy (V_O). Theoretical prediction showed that one Cu atom doped on CeO_2 (110) surface with three adjacent oxygen vacancies was the most stable structure. The oxophilic characteristic of the catalyst surface and the atomically dispersed Cu active sites are responsible for the high CH_4 selectivity.[187] Recently, Yang et al. developed a single atom Cu decorated carbon nanofiber catalyst with Cu–N_4 moieties for CO_2RR. The electrospinning membrane can be directly used as cathode for CO_2RR and exhibited nearly 100 % FE of C_1 products and a partial current density of −93 mA·cm^2 at −0.9 V_{RHE}. In particular, methanol (FE=44 %) and CO (FE=56 %) are nearly the only liquid and gas products, respectively (Figure 11c). The enhanced CO_2RR performance was ascribed to the interconnected pores and through-hole structure that facilitated the exposure of Cu single atom sites and the diffusion of CO_2 molecule. The proposed CO_2-to-CO reaction pathway on Cu–N_4 sites was similar to that on Ni–N_4 sites, where CO_2 reduced to CO via *COOH and subsequent *CO intermediates. In contrast to other studies, the desorption step of *CO intermediate was found to be slightly endergonic over Cu–N_4 sites, implying the potentiality of further reduction of *CO. The pathway of *CO reduction to methanol on Cu–N_4 was proposed in Figure 11d with moderate energy barriers. On the contrary, the higher free energy barrier (~1.88 eV) for the step of *COH to *C on Cu–N_4 sites explained why CH_3OH rather than CH_4 was the only further reduction production.[188]

Since the birth of “single-atom catalysts” in 2011, most heterogeneous SACs are decorated on various metal oxides.[189–191] However, carbon materials supported SACs are emerging and promising in the field of CO_2RR.[192] The support effect should be more significant on SACs than that on their bulk or nanoparticle counterpart as isolated active sites are directly bonded to the support.[193–194] Interestingly, Cu single atom dispersed in carbon matrix produces CH_3OH rather than CH_4,[188] while Cu single atoms supported on CeO_2 exhibited the contrary selectivity. The oxophilicity of the catalyst’s surface was believed to play a key role in determining the selectivity between methanol and methane.[195] It could be expected that the electronic structure of SACs and their CO_2RR catalytic performance can be improved by exploring the electronic metal-support interactions in the future.

An obvious difference between Cu based nanostructured catalysts and single atom Cu catalysts is that C_2 products (like C_2H_4, C_2H_6 and C_2H_5OH) which are commonly produced by Cu nanostructured catalysts are rarely reported on single atom Cu catalysts. The reason is mainly attributed to the essential C–C coupling pathway for C_2+ product is substantially blocked on isolated

Cu sites.[187-188, 196-197] Jiao et al. proposed a dual active center mechanism on a Cu-C_3N_4 (graphitic carbon nitride) model catalyst. The model catalyst was prepared by co-pyrolysis of dicyandiamide (DCDA) and $CuCl_2$ and a subsequent acid washing process. The residue Cu species in the catalyst were in the form of single atom and clusters coordinated with N atoms of C_3N_4. Interestingly, the catalyst could convert CO_2 into various C_2 product, although the Faraday efficiency was low. They proposed a new dual active center mechanism where the Cu atom functioned as an active center for carbon-anchoring intermediates (e.g., *CO, *COOH, *CHO) and the adjacent C atom of C_3N_4 acted as another active center for oxygen-anchoring intermediates (e.g., *OCH_2, *OCH_3, *O and *OH).[198] Recently, Dilan et al. reported a Cu single atom catalyst that presented a high FE of C_2 products. The Cu-N-C catalyst was synthesized by a similar mixing and pyrolysis strategy with ZIF-8, $CuCl_2$ and phenanthroline as starting materials.[118] The fitting of Fourier transformed Cu K-edge EXAFS spectrum excluded the presence of Cu clusters and revealed that the atomically dispersed Cu atoms were coordinated with four N atoms to form the Cu-N_4 sites in the carbon matrix. Under the optimized reaction conditions ($CsHCO_3$ electrolyte, CO_2 flow rate of 2.5 mL/min and potential of -1.2 V_{RHE}), a maximum FE of ethanol of 43 % with a stable current of ~16.2 mA/cm^2 was achieved on the Cu-N-C catalyst. Using CO as the feed gas further increased the FE of ethanol to 66 %, implying the important role of CO intermediate for ethanol formation. The operando XAS measurements demonstrated that the oxidation state of Cu shifted from +2 to 0 and Cu-Cu coordination appeared at potentials below -0.6 V_{RHE}. They pointed out that metallic Cu nanoparticles with an estimated size of 0.47±0.04 nm were formed during the electrolysis process. Interestingly, the in-situ formed Cu nanoparticles disappeared and Cu-N_4 sites recovered after exposing the used electrocatalyst to air. They proposed that the small Cu particles and the strong chelating capacity of the N_4 sites are responsible for the restoration of the Cu-N_4 structure.[199] Contrastingly to the well-accepted metal-N_x active sites for CO_2RR, the in-situ formed Cu nanoparticles were believed to be the active species in this work. Although the reversible structure of Cu species was also observed on Cu-phthalocyanine catalyst,[200] this phenomenon has not been observed on other heterogeneous SACs for CO_2RR.

Up to now, considerably high FE_{CO} (>90%) has been achieved for CO_2RR on various SACs. However, CO_2RR to high value products beyond CO on SACs remains a challenge. Tailoring the structure of SACs to yield highly selective electrocatalysts towards more favorable liquid products and hydrocarbons through CO_2RR may be a future direction. Cu-based SACs inherits the unique selectivity towards CO_2RR, producing hydrocarbons and alcohols as the main products. With the unique electronic structure and binding strength of intermediates, CO production can be suppressed on Cu sites. Geometrically, C-C coupling is also prohibited on isolated sites. Therefore, high selectivity towards C_1 deep reduction products may be expected on stable single Cu sites. Furthermore, to reduce CO_2 into more value C_{2+} products holds great promise with the development

of this field.[101] Atomic dual-metal sites may open up a new opportunity for CO_2RR into C_{2+} product, where more than one active center is needed.

4.2 New design to mimic the enzyme-system for CO_2RR

In nature, various enzymes are the most efficient catalysts. Many biological enzymes containing metal sites as cofactors, such as carbon monoxide dehydrogenase (CODH) and nitrogenase, play important roles in the carbon cycle and nitrogen fixation.[201-203] Mimicking the natural enzyme-system and introducing appropriate second sites which is analogous to the FeMo cofactor in nitrogenase might be a promising strategy to design the CO_2RR electrocatalysts. Constructing atomically dispersed dual-metal sites, especially the heteronuclear form, is also a promising way to tune the electronic structure and to yield a better catalytic performance.[204-205] According to the linked metals, atomically dispersed dual-metal sites can be classified into heteronuclear and homonuclear dual-metal sites.[204, 206-207] A locally distributed Pt-Co sites trapped in the defects of nitrogen-carbon base was directly observed by Zhang et al.[205] The synergetic effect of these atomic metal-metal sites regulate the electronic structure and change the charge distribution of the Pt-Co-N-C moiety, and thus endowed an enhanced selectivity towards $4e^-$ pathway of ORR. Recently, the concept of atom-pair catalyst (APC) was brought up by Li's group.[208] With the optimal Cu loading, stable Cu_1^0-Cu_1^{x+} atom-pair structures (Cu-APC) were formed on $Pd_{10}Te_3$ nanowires. The Cu-APC structure was elaborated by combination of X-ray absorption fine structure (XAFS) spectroscopy and theoretical calculation and was regarded as the active site for CO_2RR to CO. In the CO_2RR, the two Cu atoms functioned differently to promote the activation of CO_2 molecule. Although CO was still the main product in their work, it offers a great example of atomically dispersed homonuclear dual-metal sites for CO_2RR, which has the potential for more complex reduction products.

4.3 Fabrication of SACs for CO_2RR

As the single atomic sties play a key role in the catalytic process, increasing the density of isolated metal atoms on the surface of catalysts is an effective approach to boost the CO_2RR performance. Strategies are needed to increase the density of single atomic sites and, at the same time, to maintain the homogeneity of the sites and avoid the formation of any clusters or particles. In contrast to heterogeneous catalysts based on nanoparticles or nanoclusters, no homoatomic metal-metal bonds are existed in the SACs and the single metal atomic sites are anchored in the vacancies in the support by bonding to heteroatoms. Therefore, although the role of support for SACs still needs to be clarified, the support with a high content of heteroatom doping and abundant

vacancies will contribute to the high metal loading of SACs. Furthermore, it is also worth noting that the exposure and accessibility of the single atomic sites is also crucial to fulfill the 100% atomic utilization, as the single atoms that are deeply hided inside the carbon matrix or sandwiched in the graphene layers can hardly serve as active sites during the CO_2RR.

Another way to further improve the CO_2RR performance over SACs is to improve the intrinsic activity of the single atomic sites. To this end, the geometric and electronic structure of the active sites in SACs need to be elaborately tailored.

1) Single metal atoms bond to heteroatoms, such as C, N, O, and S, in the SACs. Therefore, it can be expected that regulating the type of bonded elements, the coordination number of single-atom sites, as well as the coordinated ligands are effective ways to tune the properties and catalytic performance of the SACs. Novel synthetic methods and the preparation conditions, such as the select of suitable metal precursor, ligand and support, should be carefully designed to tune the coordination environment of the single sites in SACs.[69, 95, 209] Heat treatment was an efficient way to modulate the N doping and the metal-N coordination number of SACs. With the elevated temperature, the N doping and metal-N coordination number reduced gradually, accompanied with variation in catalytic performance.[65, 86, 210]

2) Defective site created by defect engineering not only serve as intrinsic active sites for electrocatalysis, but also can anchor and trap atomic metal atoms.[210-212] The single Ni atoms embedded in the vacancies of graphene shells were probed by three-dimensional atom probe tomography. The atomic Ni species in the graphene vacancies mainly coordinated with C atoms and could facilitate the CO_2 activation and the CO desorption.[90] Zhang et al. used a defective graphene (DG) to trap Ni atoms. The atomic Ni species with different Ni-C coordination structures were successfully trapped in the graphene defects. The atomic Ni species as well as the graphene defects were deemed as an integrity to be responsible for the outstanding electrocatalytic performance.[212] Controllable formation of defects is benefit for modulating of coordination environment of SACs and constructing model catalysts for the mechanism research.

Furthermore, it is inspiring to see that some SACs have exhibited promising activity for CO_2RR at an industrial scale current density. However, there are some limitations for the application of SACs for CO_2RR in a large scale. Firstly, the catalytic performances of SACs still do not match for large-scale CO_2RR applications. Furthermore, some fundamental understandings of the SACs and their high activity in CO_2RR are still unclear. Secondly, it should be noted that many factors affect the applicability of CO_2RR in a large scale, such as the reactor configuration, the anodic reaction, the electrolyte, and the membrane, which are not included in the topic of this review. Thirdly, to advance the application of SACs for CO_2RR, more efforts are needed to investigate the stability of the SACs as the single metal sites may aggregate or leach out in CO_2RR. Finally, most reported

SACs are prepared at laboratory scale and upscaling the production to larger scales while maintaining chemical stability is a major challenge which needs to be overcome for industrial implementation. Recently, several facile methods have been developed to fabricate thermally stable SACs at large-scale. Zu et al. used a quick freeze-vacuum drying-calcination method to obtain kilogram-scale single Sn atom catalysts.[76] He et al. reported the kilogram-scale synthesis of SACs based on the ball-milling and calcination processes.[213] The novel large-scale synthesis approach of SACs are needed to advance the practical application of CO_2RR.

4.4 Unveiling the advantages and mechanism of CO_2RR on SACs

The advantages of the application of SACs in heterogeneous catalysis have been well-stated in the literature.[31, 35, 214] In the case of CO_2RR, the unique electronic structures of single metal sites are often suggested to be the reasons for their high CO_2RR performance. For instance, the electron delocalization of single Sn atomic sites led to the asymmetrical charge distribution on the isolated Sn atoms, which stabilized the $*CO_2^-$ and *COOH intermediates and facilitated the $*COOH^-$ desorption.[76] A spontaneous charge transfer from single Ni sites to CO_2 was revealed by Ni K-edge XANES spectra, indicating the readily CO_2 activation on these monovalent Ni(I) atomic sites.[75] However, the origination of these superiorities of single atomic sites remains ill-defined and is less discussed in the literatures. Through advanced experimental and computational techniques, efforts should be devoted into the fundamental advantages of SACs for CO_2RR.

SACs provide an ideal model for reaction mechanism study of CO_2RR. To date, although promising CO_2RR performance has been achieved on SACs, even at industrial-scale current density, the determination of real active sites and how these single sites boost CO_2RR are still hard tasks. Firstly, how the metal centers of SACs affect the catalytic performance of CO_2RR is not fully understood. Secondly, the metal centers are usually not isolated zero valance atoms in SACs. The coordination environment around the metal atoms strongly affect the nature of the metal center and may work cooperatively to involve into the CO_2RR process. The accurate identification of local structure is not an easy task. More attention should be paid to the coordination structures of SACs and their synergistic effects. Thirdly, unlike the metal-N molecular catalysts, more than one active center coexists in heterogeneous SACs and may take part in CO_2RR, which hampers the discovery of real active sites and the reaction mechanism of CO_2RR.

The identification of active sites, the reaction mechanism study, and the determination of structure-performance relationship are closely related to the development of advanced characterization techniques and the computational chemistry. Presently, the isolated atoms have been observed by HADDF-STEM and their local structures have been extensively discussed by X-ray absorption fine structure (XAFS) analysis. However, a powerful characterization technique

that could directly probe the coordination environment and electronic structure of the single atomic sites in SACs is still missing. On the other hand, the single atomic sites may change under real electrocatalysis conditions,[126, 200, 215] which makes the identification of the real active sites and the study of the reaction mechanism difficult. The evolution of the active sites under the working condition is rarely discussed in many literatures. The advanced in-situ characterization methods, such as in-situ XAFS, Raman, and FTIR, are of great help to provide the insight into the identification and evolution of active site for CO_2RR under working condition and the reaction mechanism. Apart from advanced characterization methods, the advances in theoretical calculations are also necessary to clarify how the structure and composition of SACs affect their CO_2RR performance and predict the activity and selectivity trends for CO_2RR.

5 Summary

Over the past several years the new frontier in heterogeneous catalysis, SACs, have witnessed explosive growth and attention. SACs are a new star in valorization of CO_2 via the CO_2RR and have exhibited comparable catalytic performance to the noble-metal benchmarks. Until recently, CO accounts for the major CO_2RR product on SACs, yet recent work shows the potential for fuel generation, including formic acid and alcohols. The formation of CO not only involves the activation of the CO_2 molecule, but also is a key step for the further reduction, thus understanding the fundamental reaction mechanism of this first step is crucial. In this review, we started with developing the fundamental understanding of the CO_2RR on SACs by both computational and experimental results. Subsequently, the heterogeneous SACs prepared by different strategies with an emphasis on their synthesis, characterization, and CO_2RR performance were highlighted. Finally, the challenge and perspectives for the research and application of SACs in CO_2RR are discussed.

Acknowledgements

M. Li and H. Wang contribute equally to this work. The authors are grateful for financial support from National Natural Science Foundation of China (No.51702046, and No.51822202), Shanghai Scientific and Technological Innovation Project (19JC1410400), Fok Ying-Tong Education Foundation of China (No. 171041), International Joint Laboratory for Advanced fiber and Low-dimension Materials (18520750400), the Program for Professor of Special Appointment (Eastern Scholar) at Shanghai Institutions of Higher Learning, DHU Distinguished Young Professor Program and Fundamental Research Funds for the Central Universities, State Key Laboratory for Modification of Chemical Fibers and Polymer Materials, Donghua University. J.C would like to thanks the financial support from Australian Research Council (CE140100012).

References

[1] B. Obama, *Science* **2017**, 355, 126.

[2] E. Dlugokencky, B. Hall, S. Montzka, G. Dutton, J. Mühle, J. Elkins, *Bull. Am. Meteorol. Soc.* **2018**, 99, S46.

[3] D. Lüthi, M. Le Floch, B. Bereiter, T. Blunier, J.-M. Barnola, U. Siegenthaler, D. Raynaud, J. Jouzel, H. Fischer, K. Kawamura, T. F. Stocker, *Nature* **2008**, 453, 379.

[4] Intergovernmental Panel on Climate Change, IPCC Special Report on the Impacts of Global Warming of 1.5 °C -Summary for Policy Makers, Incheon, **2018**

[5] S. Chu, Y. Cui, N. Liu, *Nat. Mater.* **2016**, 16, 16.

[6] J. Wu, Y. Huang, W. Ye, Y. Li, *Adv. Sci.* **2017**, 4, 1700194.

[7] J. Qiao, Y. Liu, F. Hong, J. Zhang, *Chem. Soc. Rev.* **2014**, 43, 631.

[8] M. I. Hoffert, K. Caldeira, G. Benford, D. R. Criswell, C. Green, H. Herzog, A. K. Jain, H. S. Kheshgi, K. S. Lackner, J. S. Lewis, H. D. Lightfoot, W. Manheimer, J. C. Mankins, M. E. Mauel, L. J. Perkins, M. E. Schlesinger, T. Volk, T. M. L. Wigley, *Science* **2002**, 298, 981.

[9] X. Duan, J. Xu, Z. Wei, J. Ma, S. Guo, S. Wang, H. Liu, S. Dou, *Adv. Mater.* **2017**, 29, 1701784.

[10] G. Centi, E. A. Quadrelli, S. Perathoner, *Energ. Environ, Sci.* **2013**, 6, 1711.

[11] M. B. Ross, P. De Luna, Y. Li, C.-T. Dinh, D. Kim, P. Yang, E. H. Sargent, *Nat. Catal.* **2019**, 2, 648.

[12] Q. Yang, C.-C. Yang, C.-H. Lin, H.-L. Jiang, *Angew. Chem. Int. Ed.* **2019**, 58, 3511.

[13] G. Fiorani, W. Guo, A. W. Kleij, *Green Chem.* **2015**, 17, 1375.

[14] A. Alissandratos, C. J. Easton, *Beilstein J. Org. Chem.* **2015**, 11, 2370.

[15] B. Han, X. Ou, Z. Deng, Y. Song, C. Tian, H. Deng, Y.-J. Xu, Z. Lin, *Angew. Chem. Int. Ed.* **2018**, 57, 16811.

[16] C. Li, T. Wang, B. Liu, M. Chen, A. Li, G. Zhang, M. Du, H. Wang, S. F. Liu, J. Gong, *Energ. Environ, Sci.* **2019**.

[17] Z. Liu, R. I. Masel, Q. Chen, R. Kutz, H. Yang, K. Lewinski, M. Kaplun, S. Luopa, D. R. Lutz, *J. CO2 Util.* **2016**, 15, 50.

[18] P. De Luna, R. Quintero-Bermudez, C.-T. Dinh, M. B. Ross, O. S. Bushuyev, P. Todorović, T. Regier, S. O. Kelley, P. Yang, E. H. Sargent, *Nat. Catal.* **2018**, 1, 103.

[19] D. T. Whipple, P. J. A. Kenis, *J. Phys. Chem. Lett.* **2010**, 1, 3451.

[20] J. Li, K. Chang, H. Zhang, M. He, W. A. Goddard, J. G. Chen, M.-J. Cheng, Q. Lu, *ACS Catal.* **2019**, 4709.

[21] Z. Sun, T. Ma, H. Tao, Q. Fan, B. Han, *Chem* **2017**, 3, 560.

[22] M. G. Kibria, J. P. Edwards, C. M. Gabardo, C.-T. Dinh, A. Seifitokaldani, D. Sinton, E. H. Sargent, *Adv. Mater.* **2019**, e1807166.

[23] A. Vasileff, C. Xu, Y. Jiao, Y. Zheng, S.-Z. Qiao, *Chem* **2018**, 4, 1809.

[24] Z. W. Seh, J. Kibsgaard, C. F. Dickens, I. Chorkendorff, J. K. Nørskov, T. F. Jaramillo, *Science* **2017**, 355, eaad4998.

[25] H. Takeda, C. Cometto, O. Ishitani, M. Robert, *ACS Catal.* **2017**, 7, 70.

[26] F. Franco, S. Fernández, J. Lloret-Fillol, *Current Opinion in Electrochemistry* **2019**, 15, 109.

[27] L. Zhang, Z.-J. Zhao, J. Gong, *Angew. Chem. Int. Ed.* **2017**, 56, 11326.

[28] Q. Lu, F. Jiao, *Nano Energy* **2016**, 29, 439.

[29] B. Kumar, J. P. Brian, V. Atla, S. Kumari, K. A. Bertram, R. T. White, J. M. Spurgeon, *Catal. Today* **2016**, 270, 19.

[30] X.-F. Yang, A. Wang, B. Qiao, J. Li, J. Liu, T. Zhang, *Acc. Chem. Res.* **2013**, 46, 1740.

[31] Y. Chen, S. Ji, C. Chen, Q. Peng, D. Wang, Y. Li, *Joule* **2018**, 2, 1242.

[32] B. Qiao, A. Wang, X. Yang, L. F. Allard, Z. Jiang, Y. Cui, J. Liu, J. Li, T. Zhang, *Nat. Chem.* **2011**, 3, 634.

[33] L. Zhang, Y. Ren, W. Liu, A. Wang, T. Zhang, *Natl. Sci. Rev.* **2018**, 5, 653.

[34] H. Zhang, W. Tian, X. Duan, H. Sun, S. Liu, S. Wang, *Adv. Mater.* **2019**, 1904037.

[35] A. Wang, J. Li, T. Zhang, *Nat. Rev. Chem.* **2018**, 2, 65.

[36] S. Ji, Y. Chen, X. Wang, Z. Zhang, D. Wang, Y. Li, *Chem. Rev.* **2020**. DOI: 10.1021/acs.chemrev.9b00818.

[37] S. Meshitsuka, M. Ichikawa, K. Tamaru, *J. Chem. Soc., Chem. Commun.* **1974**, 158.

[38] N. Han, Y. Wang, L. Ma, J. Wen, J. Li, H. Zheng, K. Nie, X. Wang, F. Zhao, Y. Li, J. Fan, J. Zhong, T. Wu, D. J. Miller, J. Lu, S.-T. Lee, Y. Li, *Chem* **2017**, 3, 652.

[39] Z. Zhang, J. Xiao, X.-J. Chen, S. Yu, L. Yu, R. Si, Y. Wang, S. Wang, X. Meng, Y. Wang, Z.-Q. Tian, D. Deng, *Angew. Chem. Int. Ed.* **2018**, 57, 16339.

[40] S. Ren, D. Joulié, D. Salvatore, K. Torbensen, M. Wang, M. Robert, C. P. Berlinguette, *Science* **2019**, 365, 367.

[41] X. Zhang, Z. Wu, X. Zhang, L. Li, Y. Li, H. Xu, X. Li, X. Yu, Z. Zhang, Y. Liang, H. Wang, *Nat. Commun.* **2017**, 8, 14675.

[42] S. Lin, C. S. Diercks, Y.-B. Zhang, N. Kornienko, E. M. Nichols, Y. Zhao, A. R. Paris, D. Kim, P. Yang, O. M. Yaghi, C. J. Chang, *Science* **2015**, 349, 1208.

[43] Y. Wu, J. Jiang, Z. Weng, M. Wang, D. L. J. Broere, Y. Zhong, G. W. Brudvig, Z. Feng, H. Wang, *ACS Central Sci.* **2017**, 3, 847.

[44] Y.-R. Wang, Q. Huang, C.-T. He, Y. Chen, J. Liu, F.-C. Shen, Y.-Q. Lan, *Nat. Commun.* **2018**, 9, 4466.

[45] X.-M. Hu, S. U. Pedersen, K. Daasbjerg, *Current Opinion in Electrochemistry* **2019**, 15, 148.

[46] J. Han, P. An, S. Liu, X. Zhang, D. Wang, Y. Yuan, J. Guo, X. Qiu, K. Hou, L. Shi, Y. Zhang, S. Zhao, C. Long, Z. Tang, *Angew. Chem. Int. Ed.* **2019**, 58, 12711.

[47] A. S. Varela, N. Ranjbar Sahraie, J. Steinberg, W. Ju, H.-S. Oh, P. Strasser, *Angew. Chem. Int. Ed.* **2015**, 54, 10758.

[48] D. W. Stephan, *Acc. Chem. Res.* **2015**, 48, 306.

[49] X. Yan, D. Liu, H. Cao, F. Hou, J. Liang, S. X. Dou, *Small Methods* **2019**, 3, 1800501.

[50] Q. Qin, T. Heil, M. Antonietti, M. Oschatz, *Small Methods* **2018**, 2, 1800202.

[51] F. Pan, H. Zhang, K. Liu, D. Cullen, K. More, M. Wang, Z. Feng, G. Wang, G. Wu, Y. Li, *ACS Catal.* **2018**, 8, 3116.

[52] Y. Y. Birdja, E. Pérez-Gallent, M. C. Figueiredo, A. J. Göttle, F. Calle-Vallejo, M. T. M. Koper, *Nat. Energy* **2019**, 4, 732.

[53] W. Zhang, Y. Hu, L. Ma, G. Zhu, Y. Wang, X. Xue, R. Chen, S. Yang, Z. Jin, *Adv. Sci.* **2018**, 5, 1700275.

[54] C. Long, X. Li, J. Guo, Y. Shi, S. Liu, Z. Tang, *Small Methods* **2018**, 0, 1800369.

[55] D. Gao, R. M. Arán-Ais, H. S. Jeon, B. Roldan Cuenya, *Nat. Catal.* **2019**, 2, 198.

[56] Y. Zheng, A. Vasileff, X. Zhou, Y. Jiao, M. Jaroniec, S.-Z. Qiao, *J. Am. Chem. Soc.* **2019**, 141, 7646.

[57] H. Xie, T. Wang, J. Liang, Q. Li, S. Sun, *Nano Today* **2018**, 21, 41.

[58] J. Durst, A. Rudnev, A. Dutta, Y. Fu, J. Herranz, V. Kaliginedi, A. Kuzume, A. A. Permyakova, Y. Paratcha, P. Broekmann, T. J. Schmidt, *CHIMIA International Journal for Chemistry* **2015**, 69, 769.

[59] C. Chen, J. F. Khosrowabadi Kotyk, S. W. Sheehan, *Chem* **2018**, 4, 2571.

[60] Y. Cheng, S. Yang, S. P. Jiang, S. Wang, *Small Methods* **2019**, 3, 1800440.

[61] C. Yan, L. Lin, G. Wang, X. Bao, *Chinese J. Catal.* **2019**, 40, 23.

[62] A. S. Varela, W. Ju, P. Strasser, *Adv. Energy. Mater.* **2018**, 8, 1703614.

[63] C. Zhang, S. Yang, J. Wu, M. Liu, S. Yazdi, M. Ren, J. Sha, J. Zhong, K. Nie, A. S. Jalilov, Z. Li, H. Li, B. I. Yakobson, Q. Wu, E. Ringe, H. Xu, P. M. Ajayan, J. M. Tour, *Adv. Energy. Mater.* **2018**, 8, 1703487.

[64] T. Sheng, S.-G. Sun, *Chem. Phys. Lett.* **2017**, 688, 37.

[65] X. Wang, Z. Chen, X. Zhao, T. Yao, W. Chen, R. You, C. Zhao, G. Wu, J. Wang, W. Huang, J. Yang, X. Hong, S. Wei, Y. Wu, Y. Li, *Angew. Chem. Int. Ed.* **2018**, 57, 1944.

[66] A. S. Varela, M. Kroschel, N. D. Leonard, W. Ju, J. Steinberg, A. Bagger, J. Rossmeisl, P. Strasser, *ACS Energy Lett.* **2018**, 3, 812.

[67] J. Shen, M. J. Kolb, A. J. Göttle, M. T. M. Koper, *J. Phys. Chem. C* **2016**, 120, 15714.

[68] K. Leung, I. M. B. Nielsen, N. Sai, C. Medforth, J. A. Shelnutt, *J. Phys. Chem. A* **2010**, 114, 10174.

[69] J. Gu, C.-S. Hsu, L. Bai, H. M. Chen, X. Hu, *Science* **2019**, 364, 1091.

[70] F. Pan, W. Deng, C. Justiniano, Y. Li, *Appl. Catal. B: Environ.* **2018**, 226, 463.

[71] S. Zhu, T. Li, W.-B. Cai, M. Shao, *ACS Energy Lett.* **2019**, 4, 682.

[72] N. Heidary, K. H. Ly, N. Kornienko, *Nano Lett.* **2019**, 19, 4817.

[73] A. Wuttig, C. Liu, Q. Peng, M. Yaguchi, C. H. Hendon, K. Motobayashi, S. Ye, M. Osawa, Y. Surendranath, *ACS Central Sci.* **2016**, 2, 522.

[74] S. Zhu, B. Jiang, W.-B. Cai, M. Shao, *J. Am. Chem. Soc.* **2017**, 139, 15664.

[75] H. B. Yang, S.-F. Hung, S. Liu, K. Yuan, S. Miao, L. Zhang, X. Huang, H.-Y. Wang, W. Cai, R. Chen, J. Gao, X. Yang, W. Chen, Y. Huang, H. M. Chen, C. M. Li, T. Zhang, B. Liu, *Nat. Energy* **2018**, 3, 140.

[76] X. Zu, X. Li, W. Liu, Y. Sun, J. Xu, T. Yao, W. Yan, S. Gao, C. Wang, S. Wei, Y. Xie, *Adv. Mater.* **2019**, 31, 1808135.

[77] T. Shinagawa, A. T. Garcia-Esparza, K. Takanabe, *Sci, Rep.* **2015**, 5, 13801.

[78] K. Jiang, S. Siahrostami, T. Zheng, Y. Hu, S. Hwang, E. Stavitski, Y. Peng, J. Dynes, M. Gangisetty, D. Su, K. Attenkofer, H. Wang, *Energ. Environ, Sci.* **2018**, 11, 893.

[79] W. Ren, X. Tan, W. Yang, C. Jia, S. Xu, K. Wang, S. C. Smith, C. Zhao, *Angew. Chem. Int. Ed.* **2019**, 58, 6972.

[80] W. Ju, A. Bagger, G.-P. Hao, A. S. Varela, I. Sinev, V. Bon, B. Roldan Cuenya, S. Kaskel, J. Rossmeisl, P. Strasser, *Nat. Commun.* **2017**, 8, 944.

[81] H. A. Hansen, J. B. Varley, A. A. Peterson, J. K. Nørskov, *J. Phys. Chem. Lett.* **2013**, 4, 388.

[82] Z. Wang, J. Zhao, Q. Cai, *Phys. Chem. Chem. Phys.* **2017**, 19, 23113.

[83] V. Tripkovic, M. Vanin, M. Karamad, M. E. Björketun, K. W. Jacobsen, K. S. Thygesen, J. Rossmeisl, *J. Phys. Chem. C* **2013**, 117, 9187.

[84] A. Bagger, W. Ju, A. S. Varela, P. Strasser, J. Rossmeisl, *Catal. Today* **2017**, 288, 74.

[85] X. Li, W. Bi, M. Chen, Y. Sun, H. Ju, W. Yan, J. Zhu, X. Wu, W. Chu, C. Wu, Y. Xie, *J. Am. Chem. Soc.* **2017**, 139, 14889.

[86] Y. Pan, R. Lin, Y. Chen, S. Liu, W. Zhu, X. Cao, W. Chen, K. Wu, W.-C. Cheong, Y. Wang, L. Zheng, J. Luo, Y. Lin, Y. Liu, C. Liu, J. Li, Q. Lu, X. Chen, D. Wang, Q. Peng, C. Chen, Y. Li, *J. Am. Chem. Soc.* **2018**, 140, 4218.

[87] C. Yan, H. Li, Y. Ye, H. Wu, F. Cai, R. Si, J. Xiao, S. Miao, S. Xie, F. Yang, Y. Li, G. Wang, X. Bao, *Energ. Environ, Sci.* **2018**, 11, 1204.

[88] Z. Geng, Y. Cao, W. Chen, X. Kong, Y. Liu, T. Yao, Y. Lin, *Appl. Catal. B: Environ.* **2019**, 240, 234.

[89] J. Yang, Z. Qiu, C. Zhao, W. Wei, W. Chen, Z. Li, Y. Qu, J. Dong, J. Luo, Z. Li, Y. Wu, *Angew. Chem. Int. Ed.* **2018**, 57, 14095.

[90] K. Jiang, S. Siahrostami, A. J. Akey, Y. Li, Z. Lu, J. Lattimer, Y. Hu, C. Stokes, M. Gangishetty, G. Chen, Y. Zhou, W. Hill, W.-B. Cai, D. Bell, K. Chan, J. K. Nørskov, Y. Cui, H. Wang, *Chem* **2017**, 3, 950.

[91] S. Back, J. Lim, N.-Y. Kim, Y.-H. Kim, Y. Jung, *Chem. Sci.* **2017**, 8, 1090.

[92] Q. Xu, C. Guo, S. Tian, J. Zhang, W. Chen, W.-C. Cheong, L. Gu, L. Zheng, J. Xiao, Q. Liu, B. Li, D. Wang, Y. Li, *Sci. China Mater*. 2020, DOI: 10.1007/s40843-020-1334-6.

[93] Y. Li, Z.-S. Wu, P. Lu, X. Wang, W. Liu, Z. Liu, J. Ma, W. Ren, Z. Jiang, X. Bao, *Adv. Sci.* **2020**, 7, 1903089.

[94] Y. Ren, Y. Tang, L. Zhang, X. Liu, L. Li, S. Miao, D. Sheng Su, A. Wang, J. Li, T. Zhang, *Nat. Commun.* **2019**, 10, 4500.

[95] L. Wang, M.-X. Chen, Q.-Q. Yan, S.-L. Xu, S.-Q. Chu, P. Chen, Y. Lin, H.-W. Liang, *Science Advances* **2019**, 5, eaax6322.

[96] J. Wan, W. Chen, C. Jia, L. Zheng, J. Dong, X. Zheng, Y. Wang, W. Yan, C. Chen, Q. Peng, D. Wang, Y. Li, *Adv. Mater.* **2018**, 30, 1705369.

[97] X. Li, H. Rong, J. Zhang, D. Wang, Y. Li, *Nano Res.* **2020**. DOI: 10.1007/s12274-020-2755-3.

[98] C. Shi, H. A. Hansen, A. C. Lausche, J. K. Nørskov, *Phys. Chem. Chem. Phys.* **2014**, 16, 4720.

[99] D. Kim, C. Xie, N. Becknell, Y. Yu, M. Karamad, K. Chan, E. J. Crumlin, J. K. Nørskov, P. Yang, *J. Am. Chem. Soc.* **2017**, 139, 8329.

[100] E. Zhang, T. Wang, K. Yu, J. Liu, W. Chen, A. Li, H. Rong, R. Lin, S. Ji, X.-S. Zheng, Y. Wang, L. Zheng, C. Chen, D. Wang, J. Zhang, Y. Li, *J. Am. Chem. Soc.* **2019**.

[101] O. S. Bushuyev, P. De Luna, C. T. Dinh, L. Tao, G. Saur, J. van de Lagemaat, S. O. Kelley, E. H. Sargent, *Joule* **2018**, 2, 825.

[102] H. Yoshio, K. Katsuhei, S. Shin, *Chem. Lett.* **1985**, 14, 1695.

[103] J. Choi, T. M. Benedetti, R. Jalili, A. Walker, G. G. Wallace, D. L. Officer, *Chem. -Eur. J.* **2016**, 22, 14158.

[104] C. Costentin, S. Drouet, M. Robert, J.-M. Savéant, *Science* **2012**, 338, 90.

[105] Z. N. Zahran, E. A. Mohamed, Y. Naruta, *Sci, Rep.* **2016**, 6, 24533.

[106] W. Zhu, R. Michalsky, Ö. Metin, H. Lv, S. Guo, C. J. Wright, X. Sun, A. A. Peterson, S. Sun, *J. Am. Chem. Soc.* **2013**, 135, 16833.

[107] S. Liu, H. Tao, L. Zeng, Q. Liu, Z. Xu, Q. Liu, J.-L. Luo, *J. Am. Chem. Soc.* **2017**, 139, 2160.

[108] G. Wan, G. Zhang, X.-M. Lin, *Adv. Mater.* **2020**, 32, 1905548.

[109] M. Liu, L. Wang, K. Zhao, S. Shi, Q. Shao, L. Zhang, X. Sun, Y. Zhao, J. Zhang, *Energ. Environ. Sci.* **2019**, 12, 2890.

[110] H. T. Chung, D. A. Cullen, D. Higgins, B. T. Sneed, E. F. Holby, K. L. More, P. Zelenay, *Science* **2017**, 357, 479.

[111] N. R. Sahraie, U. I. Kramm, J. Steinberg, Y. Zhang, A. Thomas, T. Reier, J.-P. Paraknowitsch, P. Strasser, *Nat. Commun.* **2015**, 6, 8618.

[112] U. Martinez, S. Komini Babu, E. F. Holby, H. T. Chung, X. Yin, P. Zelenay, *Adv. Mater.* **2019**, 31, 1806545.

[113] X.-M. Hu, H. H. Hval, E. T. Bjerglund, K. J. Dalgaard, M. R. Madsen, M.-M. Pohl, E. Welter, P. Lamagni, K. B. Buhl, M. Bremholm, M. Beller, S. U. Pedersen, T. Skrydstrup, K. Daasbjerg, *ACS Catal.* **2018**, 8, 6255.

[114] G. Wan, P. Yu, H. Chen, J. Wen, C.-j. Sun, H. Zhou, N. Zhang, Q. Li, W. Zhao, B. Xie, T. Li, J. Shi, *Small* **2018**, 14, 1704319.

[115] J.-J. Shi, X.-M. Hu, M. R. Madsen, P. Lamagni, E. T. Bjerglund, S. U. Pedersen, T. Skrydstrup, K. Daasbjerg, *ACS Applied Nano Materials* **2018**, 1, 3608.

[116] X. Fu, N. Li, B. Ren, G. Jiang, Y. Liu, F. M. Hassan, D. Su, J. Zhu, L. Yang, Z. Bai, Z. P. Cano, A. Yu, Z. Chen, *Adv. Energy. Mater.* **2019**, 9, 1803737.

[117] Y. Cheng, S. Zhao, H. Li, S. He, J.-P. Veder, B. Johannessen, J. Xiao, S. Lu, J. Pan, M. F. Chisholm, S.-Z. Yang, C. Liu, J. G. Chen, S. P. Jiang, *Appl. Catal. B: Environ.* **2019**, 243, 294.

[118] T. N. Huan, N. Ranjbar, G. Rousse, M. Sougrati, A. Zitolo, V. Mougel, F. Jaouen, M. Fontecave, *ACS Catal.* **2017**, 7, 1520.

[119] B. Kumar, M. Asadi, D. Pisasale, S. Sinha-Ray, B. A. Rosen, R. Haasch, J. Abiade, A. L. Yarin, A. Salehi-Khojin, *Nat. Commun.* **2013**, 4, 2819.

[120] P. P. Sharma, J. Wu, R. M. Yadav, M. Liu, C. J. Wright, C. S. Tiwary, B. I. Yakobson, J. Lou, P. M. Ajayan, X.-D. Zhou, *Angew. Chem. Int. Ed.* **2015**, 54, 13701.

[121] J. Wu, S. Ma, J. Sun, J. I. Gold, C. Tiwary, B. Kim, L. Zhu, N. Chopra, I. N. Odeh, R. Vajtai, A. Z. Yu, R. Luo, J. Lou, G. Ding, P. J. A. Kenis, P. M. Ajayan, *Nat. Commun.* **2016**, 7, 13869.

[122] J. Xu, Y. Kan, R. Huang, B. Zhang, B. Wang, K.-H. Wu, Y. Lin, X. Sun, Q. Li, G. Centi, D. Su, *ChemSusChem* **2016**, 9, 1085.

[123] D. M. Fernandes, A. F. Peixoto, C. Freire, *Dalton Trans.* **2019**, 48, 13508.

[124] H.-J. Yang, X. Zhang, Y.-H. Hong, H. M. K. Sari, Z.-Y. Zhou, S.-G. Sun, X.-F. Li, *ChemSusChem* **2019**, 12, 3988.

[125] K. Artyushkova, I. Matanovic, B. Halevi, P. Atanassov, *J. Phys. Chem. C* **2017**, 121, 2836.

[126] N. Leonard, W. Ju, I. Sinev, J. Steinberg, F. Luo, A. S. Varela, B. Roldan Cuenya, P. Strasser, *Chem. Sci.* **2018**, 9, 5064.

[127] M. Zhang, T.-S. Wu, S. Hong, Q. Fan, Y.-L. Soo, J. Masa, J. Qiu, Z. Sun, *ACS Sustain. Chem. Eng.* **2019**, 7, 15030.

[128] J. Li, S. Chen, N. Yang, M. Deng, S. Ibraheem, J. Deng, J. Li, L. Li, Z. Wei, *Angew. Chem. Int. Ed.* **2019**, 58, 7035.

[129] Y. Cheng, S. Zhao, B. Johannessen, J.-P. Veder, M. Saunders, M. R. Rowles, M. Cheng, C. Liu, M. F. Chisholm, R. De Marco, H.-M. Cheng, S.-Z. Yang, S. P. Jiang, *Adv. Mater.* **2018**, 30, e1706287.

[130] S. Zhao, Y. Cheng, J.-P. Veder, B. Johannessen, M. Saunders, L. Zhang, C. Liu, M. F. Chisholm, R. De Marco, J. Liu, S.-Z. Yang, S. P. Jiang, *ACS Appl. Energ. Mater.* **2018**, 1, 5286.

[131] T. Zheng, K. Jiang, N. Ta, Y. Hu, J. Zeng, J. Liu, H. Wang, *Joule* **2018**, 3, 265.

[132] T. Möller, W. Ju, A. Bagger, X. Wang, F. Luo, T. Ngo Thanh, A. S. Varela, J. Rossmeisl, P. Strasser, *Energ. Environ, Sci.* **2019**, 12, 640.

[133] W. Luo, J. Zhang, M. Li, A. Züttel, *ACS Catal.* **2019**, 9, 3783.

[134] X. Jiang, F. Cai, D. Gao, J. Dong, S. Miao, G. Wang, X. Bao, *Electrochem. Commun.* **2016**, 68, 67.

[135] H. S. Jeon, I. Sinev, F. Scholten, N. J. Divins, I. Zegkinoglou, L. Pielsticker, B. R. Cuenya, *J. Am. Chem. Soc.* **2018**, 140, 9383.

[136] K. Liu, J. Wang, M. Shi, J. Yan, Q. Jiang, *Adv. Energy. Mater.* **2019**, 9, 1900276.

[137] J. Rosen, G. S. Hutchings, Q. Lu, R. V. Forest, A. Moore, F. Jiao, *ACS Catal.* **2015**, 5, 4586.

[138] Z. Chen, K. Mou, S. Yao, L. Liu, *ChemSusChem* **2018**, 11, 2944.

[139] F. Yang, P. Song, X. Liu, B. Mei, W. Xing, Z. Jiang, L. Gu, W. Xu, *Angew. Chem. Int. Ed.* **2018**, 57, 12303.

[140] H. Zhang, H. T. Chung, D. A. Cullen, S. Wagner, U. I. Kramm, K. L. More, P. Zelenay, G. Wu, *Energ. Environ, Sci.* **2019**.

[141] H. Yang, X. Chen, W.-T. Chen, Q. Wang, N. C. Cuello, A. Nafady, A. M. Al-Enizi, G. I. N. Waterhouse, G. A. Goenaga, T. A. Zawodzinski, P. E. Kruger, J. E. Clements, J. Zhang, H. Tian, S. G. Telfer, S. Ma, *ACS Nano* **2019**.

[142] H. Zhang, S. Hwang, M. Wang, Z. Feng, S. Karakalos, L. Luo, Z. Qiao, X. Xie, C. Wang, D. Su, Y. Shao, G. Wu, *J. Am. Chem. Soc.* **2017**, 139, 14143.

[143] Y. Hori, H. Wakebe, T. Tsukamoto, O. Koga, *Electrochim. Acta* **1994**, 39, 1833.

[144] I. Shoichiro, T. Takehiko, I. Kaname, *Bull. Chem. Soc. Jpn.* **1987**, 60, 2517.

[145] C. Zhao, J. Wang, *Chem. Eng. J.* **2016**, 293, 161.

[146] S. Sarfraz, A. T. Garcia-Esparza, A. Jedidi, L. Cavallo, K. Takanabe, *ACS Catal.* **2016**, 6, 2842.

[147] X. Bai, W. Chen, C. Zhao, S. Li, Y. Song, R. Ge, W. Wei, Y. Sun, *Angew. Chem. Int. Ed.* **2017**, 56, 12219.

[148] L. Fan, Z. Xia, M. Xu, Y. Lu, Z. Li, *Adv. Funct. Mater.* **2018**, 28.

[149] Y. Liu, M. Fan, X. Zhang, Q. Zhang, D. Guay, J. Qiao, *Electrochim. Acta* **2017**, 248, 123.

[150] F. Li, L. Chen, M. Xue, T. Williams, Y. Zhang, D. R. MacFarlane, J. Zhang, *Nano Energy* **2017**, 31, 270.

[151] X. Zheng, P. De Luna, F. P. García de Arquer, B. Zhang, N. Becknell, M. B. Ross, Y. Li, M. N. Banis, Y. Li, M. Liu, O. Voznyy, C. T. Dinh, T. Zhuang, P. Stadler, Y. Cui, X. Du, P. Yang, E. H. Sargent, *Joule* **2017**, 1, 794.

[152] A. Zhang, R. He, H. Li, Y. Chen, T. Kong, K. Li, H. Ju, J. Zhu, W. Zhu, J. Zeng, *Angew. Chem. Int. Ed.* **2018**, 57, 10954.

[153] W. Ju, F. Jiang, H. Ma, Z. Pan, Y.-B. Zhao, F. Pagani, D. Rentsch, J. Wang, C. Battaglia, *Adv. Energy. Mater.* **2019**, 1901514.

[154] S. Zhao, S. Li, T. Guo, S. Zhang, J. Wang, Y. Wu, Y. Chen, *Nano-Micro Lett.* **2019**, 11, 62.

[155] J. Gu, F. Héroguel, J. Luterbacher, X. Hu, *Angew. Chem. Int. Ed.* **2018**, 57, 2943.

[156] F. Lei, W. Liu, Y. Sun, J. Xu, K. Liu, L. Liang, T. Yao, B. Pan, S. Wei, Y. Xie, *Nat. Commun.* **2016**, 7, 12697.

[157] Y. Zhao, J. Liang, C. Wang, J. Ma, G. G. Wallace, *Adv. Energy. Mater.* **2018**, 8, 1702524.

[158] M. Jia, S. Hong, T.-S. Wu, X. Li, Y.-L. Soo, Z. Sun, *Chem. Commun.* **2019**, 55, 12024.

[159] P. Su, K. Iwase, S. Nakanishi, K. Hashimoto, K. Kamiya, *Small* **2016**, 12, 6083.

[160] H. Zhang, J. Li, S. Xi, Y. Du, X. Hai, J. Wang, H. Xu, G. Wu, J. Zhang, J. Lu, J. Wang, *Angew. Chem. Int. Ed.* **2019**, 58, 14871.

[161] H. Furukawa, K. E. Cordova, M. O'Keeffe, O. M. Yaghi, *Science* **2013**, 341, 1230444.

[162] P. Nugent, Y. Belmabkhout, S. D. Burd, A. J. Cairns, R. Luebke, K. Forrest, T. Pham, S. Ma, B. Space, L. Wojtas, M. Eddaoudi, M. J. Zaworotko, *Nature* **2013**, 495, 80.

[163] S. Dou, J. Song, S. Xi, Y. Du, J. Wang, Z.-F. Huang, Z. J. Xu, X. Wang, *Angew. Chem.* **2019**, 131, 4081.

[164] Y. Wang, P. Hou, Z. Wang, P. Kang, *ChemPhysChem* **2017**, 18, 3142.

[165] X. Jiang, H. Li, J. Xiao, D. Gao, R. Si, F. Yang, Y. Li, G. Wang, X. Bao, *Nano Energy* **2018**, 52, 345.

[166] A. Han, B. Wang, A. Kumar, Y. Qin, J. Jin, X. Wang, C. Yang, B. Dong, Y. Jia, J. Liu, X. Sun, *Small Methods* **2019**, 0, 1800471.

[167] T. Sun, L. Xu, D. Wang, Y. Li, *Nano Res.* **2019**, 12, 2067.

[168] Z. Liang, C. Qu, D. Xia, R. Zou, Q. Xu, *Angew. Chem. Int. Ed.* **2018**, 57, 9604.

[169] J. Wang, G. Han, L. Wang, L. Du, G. Chen, Y. Gao, Y. Ma, C. Du, X. Cheng, P. Zuo, G. Yin, *Small* **2018**, 14, 1704282.

[170] Y. Chen, S. Ji, Y. Wang, J. Dong, W. Chen, Z. Li, R. Shen, L. Zheng, Z. Zhuang, D. Wang, Y. Li, *Angew. Chem. Int. Ed.* **2017**, 56, 6937.

[171] Z. Geng, Y. Liu, X. Kong, P. Li, K. Li, Z. Liu, J. Du, M. Shu, R. Si, J. Zeng, *Adv. Mater.* **2018**, 30, 1803498.

[172] H. Tao, C. Choi, L.-X. Ding, Z. Jiang, Z. Han, M. Jia, Q. Fan, Y. Gao, H. Wang, A. W. Robertson, S. Hong, Y. Jung, S. Liu, Z. Sun, *Chem* **2019**, 5, 204.

[173] X. Song, H. Zhang, Y. Yang, B. Zhang, M. Zuo, X. Cao, J. Sun, C. Lin, X. Li, Z. Jiang, *Adv. Sci.* **2018**, 5, 1800177.

[174] C. Zhao, X. Dai, T. Yao, W. Chen, X. Wang, J. Wang, J. Yang, S. Wei, Y. Wu, Y. Li, *J. Am. Chem. Soc.* **2017**, 139, 8078.

[175] L. Yang, D. Cheng, H. Xu, X. Zeng, X. Wan, J. Shui, Z. Xiang, D. Cao, *Proc. Natl. Acad. Sci.* **2018**, 115, 6626.

[176] Y. Ye, F. Cai, H. Li, H. Wu, G. Wang, Y. Li, S. Miao, S. Xie, R. Si, J. Wang, X. Bao, *Nano Energy* **2017**, 38, 281.

[177] S. Wei, A. Li, J.-C. Liu, Z. Li, W. Chen, Y. Gong, Q. Zhang, W.-C. Cheong, Y. Wang, L. Zheng, H. Xiao, C. Chen, D. Wang, Q. Peng, L. Gu, X. Han, J. Li, Y. Li, *Nat. Nanotechnol.* **2018**, 13, 856.

[178] N. Han, Y. Wang, H. Yang, J. Deng, J. Wu, Y. Li, Y. Li, *Nat. Commun.* **2018**, 9, 1320.

[179] H. Yang, N. Han, J. Deng, J. Wu, Y. Wang, Y. Hu, P. Ding, Y. Li, Y. Li, J. Lu, *Adv. Energy. Mater.* **2018**, 8, 1801536.

[180] K. P. Kuhl, E. R. Cave, D. N. Abram, T. F. Jaramillo, *Energ. Environ, Sci.* **2012**, 5, 7050.

[181] P. Huang, M. Cheng, H. Zhang, M. Zuo, C. Xiao, Y. Xie, *Nano Energy* **2019**, 61, 428.

[182] Y. C. Li, Z. Wang, T. Yuan, D.-H. Nam, M. Luo, J. Wicks, B. Chen, J. Li, F. Li, F. P. G. de Arquer, Y. Wang, C.-T. Dinh, O. Voznyy, D. Sinton, E. H. Sargent, *J. Am. Chem. Soc.* **2019**, 141, 8584.

[183] L. Lu, X. Sun, J. Ma, D. Yang, H. Wu, B. Zhang, J. Zhang, B. Han, *Angew. Chem. Int. Ed.* **2018**, 57, 14149.

[184] T.-T. Zhuang, Y. Pang, Z.-Q. Liang, Z. Wang, Y. Li, C.-S. Tan, J. Li, C. T. Dinh, P. De Luna, P.-L. Hsieh, T. Burdyny, H.-H. Li, M. Liu, Y. Wang, F. Li, A. Proppe, A. Johnston, D.-H. Nam, Z.-Y. Wu, Y.-R. Zheng, A. H. Ip, H. Tan, L.-J. Chen, S.-H. Yu, S. O. Kelley, D. Sinton, E. H. Sargent, *Nat. Catal.* **2018**.

[185] Y. Li, F. Cui, M. B. Ross, D. Kim, Y. Sun, P. Yang, *Nano Lett.* **2017**, 17, 1312.

[186] Z. Zhao, X. Peng, X. Liu, X. Sun, J. Shi, L. Han, G. Li, J. Luo, *J. Mater. Chem. A* **2017**, 5, 20239.

[187] Y. Wang, Z. Chen, P. Han, Y. Du, Z. Gu, X. Xu, G. Zheng, *ACS Catal.* **2018**, 8, 7113.

[188] H. Yang, Y. Wu, G. Li, Q. Lin, Q. Hu, Q. Zhang, J. Liu, C. He, *J. Am. Chem. Soc.* **2019**.

[189] J. Lin, A. Wang, B. Qiao, X. Liu, X. Yang, X. Wang, J. Liang, J. Li, J. Liu, T. Zhang, *J. Am. Chem. Soc.* **2013**, 135, 15314.

[190] Z. Zhang, Y. Zhu, H. Asakura, B. Zhang, J. Zhang, M. Zhou, Y. Han, T. Tanaka, A. Wang, T. Zhang, N. Yan, *Nat. Commun.* **2017**, 8, 16100.

[191] P. Liu, Y. Zhao, R. Qin, S. Mo, G. Chen, L. Gu, D. M. Chevrier, P. Zhang, Q. Guo, D. Zang, B. Wu, G. Fu, N. Zheng, *Science* **2016**, 352, 797.

[192] Y. Peng, B. Lu, S. Chen, *Adv. Mater.* **2018**, 30, 1801995.

[193] J. Li, Q. Guan, H. Wu, W. Liu, Y. Lin, Z. Sun, X. Ye, X. Zheng, H. Pan, J. Zhu, S. Chen, W. Zhang, S. Wei, J. Lu, *J. Am. Chem. Soc.* **2019**, 141, 14515.

[194] G. Zhao, H. Liu, J. Ye, *Nano Today* **2018**, 19, 108.

[195] K. P. Kuhl, T. Hatsukade, E. R. Cave, D. N. Abram, J. Kibsgaard, T. F. Jaramillo, *J. Am. Chem. Soc.* **2014**, 136, 14107.

[196] K. Jiang, R. B. Sandberg, A. J. Akey, X. Liu, D. C. Bell, J. K. Nørskov, K. Chan, H. Wang, *Nat. Catal.* **2018**, 1, 111.

[197] D. Kim, C. S. Kley, Y. Li, P. Yang, *Proc. Natl. Acad. Sci.* **2017**, 114, 10560.

[198] Y. Jiao, Y. Zheng, P. Chen, M. Jaroniec, S.-Z. Qiao, *J. Am. Chem. Soc.* **2017**, 139, 18093.

[199] M. Fontecave, D. Karapinar, N. H. Tran, N. Ranjbar Sahraie, J. Li, N. Touati, S. Zanna, D. Taverna, L. H. Galvão Tizei, A. Zitolo, F. Jaouen, V. Mougel, D. Wakerley, *Angew. Chem. Int. Ed.* **2019**, 58, 15098.

[200] Z. Weng, Y. Wu, M. Wang, J. Jiang, K. Yang, S. Huo, X.-F. Wang, Q. Ma, G. W. Brudvig, V. S. Batista, Y. Liang, Z. Feng, H. Wang, *Nat. Commun.* **2018**, 9, 415.

[201] S. L. Foster, S. I. P. Bakovic, R. D. Duda, S. Maheshwari, R. D. Milton, S. D. Minteer, M. J. Janik, J. N. Renner, L. F. Greenlee, *Nat. Catal.* **2018**, 1, 490.

[202] Y. Kung, C. L. Drennan, *Curr. Opin. Chem. Biol.* **2011**, 15, 276.

[203] R. D. Milton, S. Abdellaoui, N. Khadka, D. R. Dean, D. Leech, L. C. Seefeldt, S. D. Minteer, *Energ. Environ. Sci.* **2016**, 9, 2550.

[204] F. Li, X. Liu, Z. Chen, *Small Methods* **2019**, 3, 1800480.

[205] L. Zhang, J. M. T. A. Fischer, Y. Jia, X. Yan, W. Xu, X. Wang, J. Chen, D. Yang, H. Liu, L. Zhuang, M. Hankel, D. J. Searles, K. Huang, S. Feng, C. L. Brown, X. Yao, *J. Am. Chem. Soc.* **2018**, 140, 10757.

[206] T. Chao, X. Luo, W. Chen, B. Jiang, J. Ge, Y. Lin, G. Wu, X. Wang, Y. Hu, Z. Zhuang, Y. Wu, X. Hong, Y. Li, *Angew. Chem. Int. Ed.* **2017**, 56, 16047.

[207] H. Yan, Y. Lin, H. Wu, W. Zhang, Z. Sun, H. Cheng, W. Liu, C. Wang, J. Li, X. Huang, T. Yao, J. Yang, S. Wei, J. Lu, *Nat. Commun.* **2017**, 8, 1070.

[208] J. Jiao, R. Lin, S. Liu, W.-C. Cheong, C. Zhang, Z. Chen, Y. Pan, J. Tang, K. Wu, S.-F. Hung, H. M. Chen, L. Zheng, Q. Lu, X. Yang, B. Xu, H. Xiao, J. Li, D. Wang, Q. Peng, C. Chen, Y. Li, *Nat. Chem.* **2019**, 11, 222.

[209] Z. Yang, Y. Wang, M. Zhu, Z. Li, W. Chen, W. Wei, T. Yuan, Y. Qu, Q. Xu, C. Zhao, X. Wang, P. Li, Y. Li, Y. Wu, Y. Li, *ACS Catal.* **2019**, 9, 2158.

[210] Y. Jia, L. Zhang, A. Du, G. Gao, J. Chen, X. Yan, C. L. Brown, X. Yao, *Adv. Mater.* **2016**, 28, 9532.

[211] Y. Jia, L. Zhang, L. Zhuang, H. Liu, X. Yan, X. Wang, J. Liu, J. Wang, Y. Zheng, Z. Xiao, E. Taran, J. Chen, D. Yang, Z. Zhu, S. Wang, L. Dai, X. Yao, *Nat. Catal.* **2019**, 2, 688.

[212] L. Zhang, Y. Jia, G. Gao, X. Yan, N. Chen, J. Chen, M. T. Soo, B. Wood, D. Yang, A. Du, X. Yao, *Chem* **2018**, 4, 285.

[213] X. He, Y. Deng, Y. Zhang, Q. He, D. Xiao, M. Peng, Y. Zhao, H. Zhang, R. Luo, T. Gan, H. Ji, D. Ma, *Cell Reports Physical Science* **2019**, 100004.

[214] C. Zhu, S. Fu, Q. Shi, D. Du, Y. Lin, *Angew. Chem. Int. Ed.* **2017**, 56, 13944.

[215] L. Cao, Q. Luo, W. Liu, Y. Lin, X. Liu, Y. Cao, W. Zhang, Y. Wu, J. Yang, T. Yao, S. Wei, *Nat. Catal.* **2019**, 2, 134.

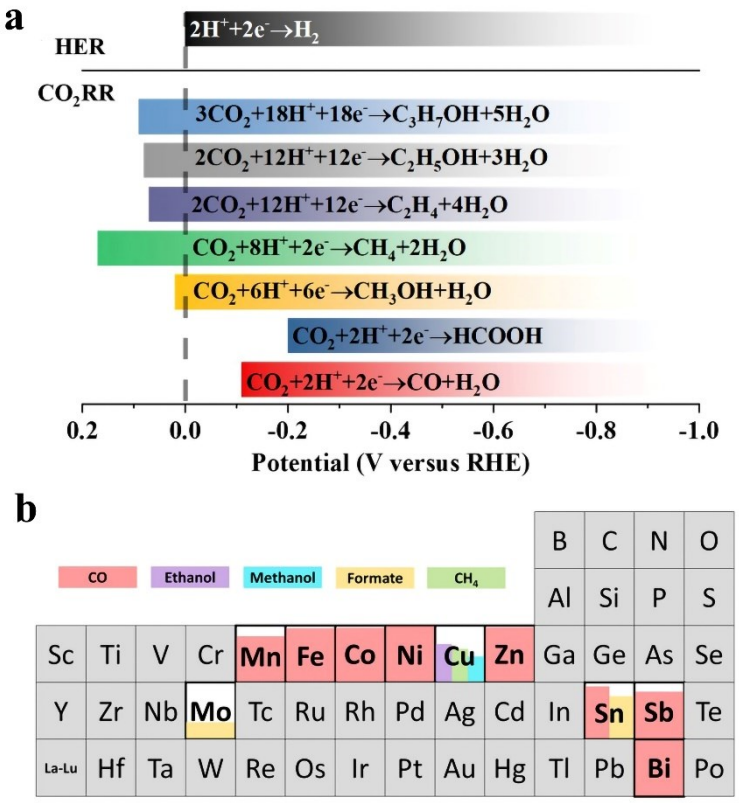

Figure 1. (a) The thermodynamic potentials for the major CO_2RR half-reactions and the competing HER in aqueous electrolyte under standard conditions (1.0 atm, 25 °C and pH=7.0). (b) The reported metals that are used as single atomic sites for CO_2RR (the vertical length of the bar represents the best Faradaic Efficiency in the literature for the color coded product).

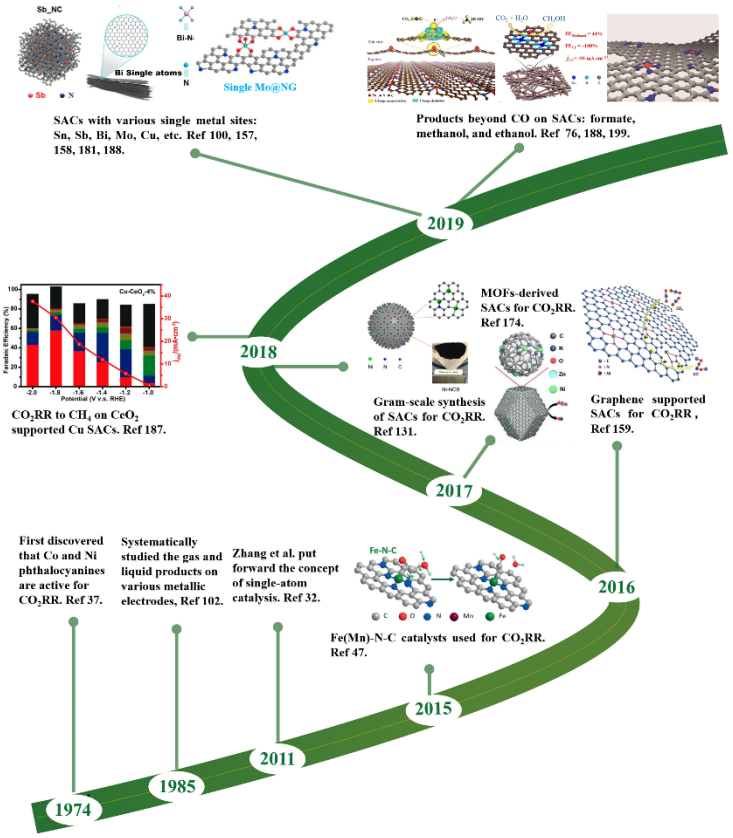

Figure 2. A brief history of catalysts for CO_2RR and the recent progress of SACs for CO_2RR. In 2011, Zhang et al. put forward the concept of the single-atom catalyst by catalyzing CO oxidation by Pt_1/FeO_x catalyst.[32] In 2015-2017, pyrolyzed M-N-C catalysts, graphene supported SACs, and MOFs-derived SACs have been synthesized and applied to CO_2RR.[47, 159, 174] Subsequently, SACs with different central metals and products beyond CO have been developed for CO_2RR.[76, 100, 158, 187-188, 199]

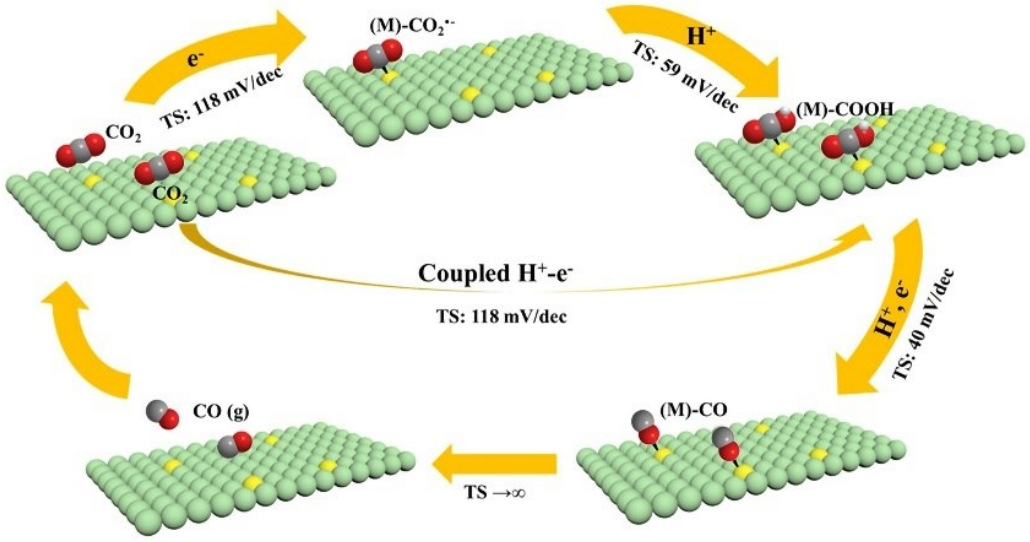

Figure 3. The proposed reaction pathways of CO_2RR to CO and the estimated Tafel slope (TS) values for each possible rate-determining step.[69]

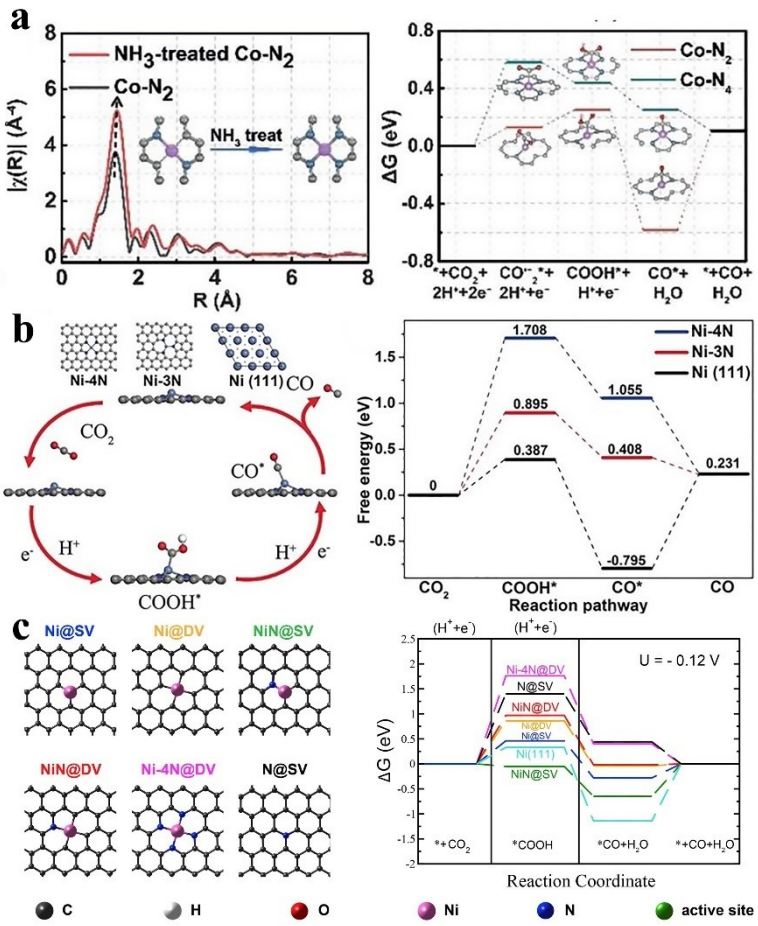

Figure 4. Effect of the coordination environment on SACs for CO_2RR. (a) The transform of Co-N_2 to Co-N_4 by NH_3-treatment by EXAFS analysis (Right) and the free energy diagrams for CO_2RR to CO on Co-N_2 and Co-N_4 (Left). Reproduced with permission.[65] Copyright 2018, Wiley-VCH. (b) Different coordination configurations of Ni atoms in graphene (Right) and the free energy diagram for CO_2 to CO on different Ni atomic sites at the equilibrium potential (Left). Reproduced with permission.[90] Copyright 2017, Elsevier. (c) (Right) Models of constructed structure for Ni SAs (Ni-4N and Ni-3N) and Ni NPs (Ni(111)) catalysts and the proposed CO_2RR pathway. (Left) Free energy diagram for CO_2 to CO at U=0 V_{RHE} on the proposed structures. Reproduced with permission.[89] Copyright 2018, Wiley-VCH.

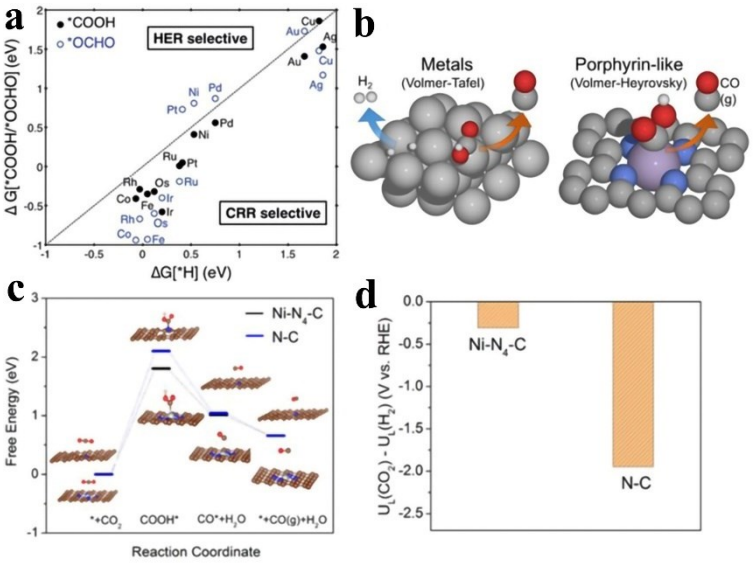

Figure 5. The HER suppression on SACs during CO_2RR. (a) Free energy change of the first protonation step in CO_2RR and HER on various SACs. Catalysts below the dotted parity line are CO_2RR selective. Reproduced with permission.[91] Copyright 2017, The Royal Society of Chemistry. (b) The porphyrin-like structure forces CO_2RR or HER to proceed via a Volmer-Heyrowsky mechanism. Reproduced with permission.[84] Copyright 2017, Elsevier. (c) The free energy diagram for the CO formation and (d) the difference in limiting potentials for CO_2RR and HER on Ni-N_4-C sites. c,d) Reproduced with permission.[85] Copyright 2017, American Chemical Society.

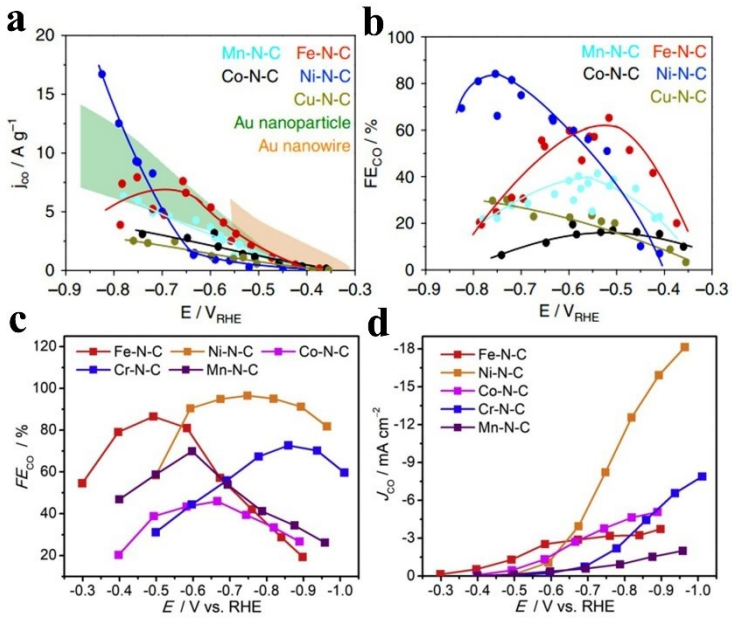

Figure 6 CO_2RR performance of pyrolyzed M-N-C catalysts. FE_{CO} (a) and catalyst mass-normalized CO partial currents (b) for the five M–N–C catalysts compared to state-of-art Au catalysts. a,b) Reproduced with permission.[80] Copyright 2017, Springer Nature. FE_{CO} (c) and CO partial current densities (d) for M-N-C. c,d) Reproduced with permission.[70] Copyright 2018, Elsevier.

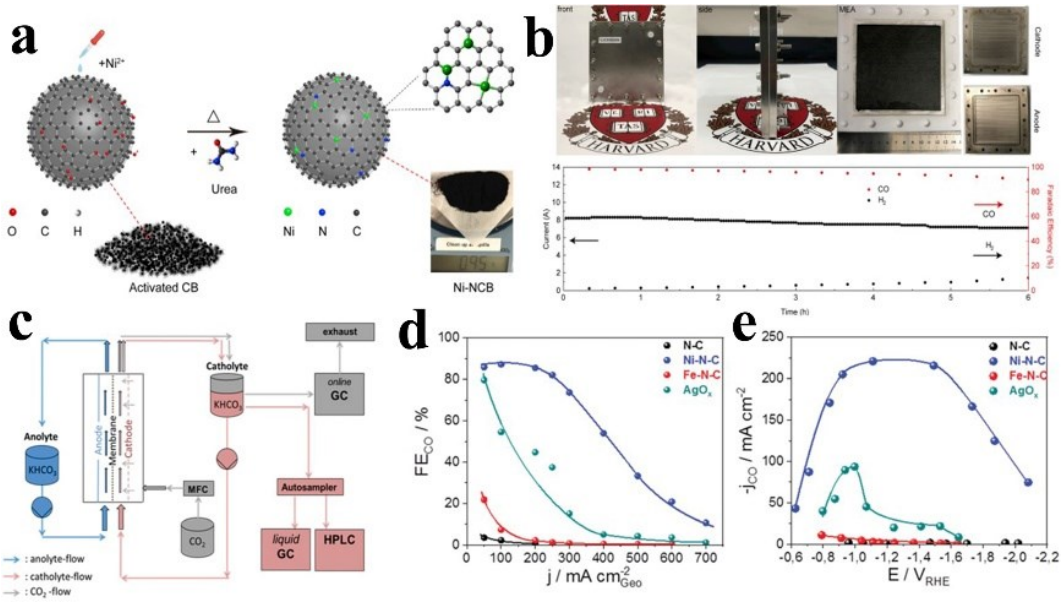

Figure 7. CO_2RR performance on SACs at industrial-scale current density. (a) Schematic of the synthesis of gram-scale single atom Ni-NCB catalyst. (b) Photographs of membrane electrode assembly system and long-term electrolysis under a full-cell voltage of 2.8 V. a,b) Reproduced with permission.[131] Copyright 2019, Elsevier. (c) CO_2 electrolyzer flow cell set up. (d) FE_{CO} efficiency as a function of the applied electrolyzer current density. (e) CO partial current density as a function of iR-corrected CO_2 electrode potentials. c–e) Reproduced with permission.[132] Copyright 2019, The Royal Society of Chemistry.

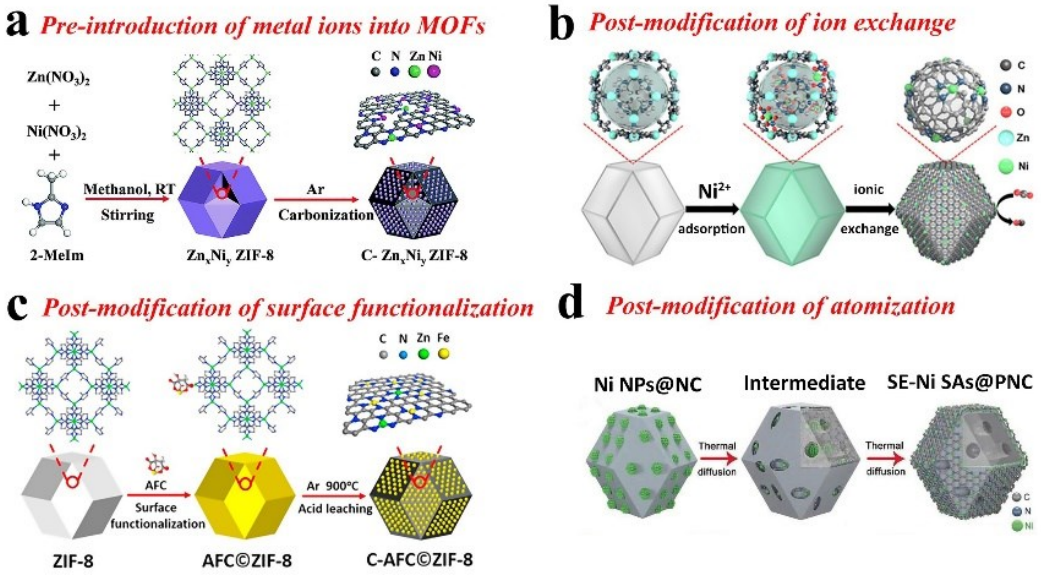

Figure 8. MOFs derived SACs for CO_2RR. MOFs derived SACs by pre-introduction strategy. (a) C-Zn_xNi_y ZIF-8 catalysts. Reproduced with permission.[87] Copyright 2018, The Royal Society of Chemistry. MOFs derived SACs by post-modification strategy. (b) Ni SAs/N-C catalyst. Reproduced with permission.[174] Copyright 2017, American Chemical Society. (c) C-AFC©ZIF-8 catalyst. Reproduced with permission.[176] Copyright 2017, Elsevier. (d) SE-Ni SAs@PNC catalyst. Reproduced with permission.[89] Copyright 2018, Wiley-VCH.

Pyrolyzed M-N-C catalysts	Graphene supported SACs	MOFs-derived SACs
✓ *Low-cost and diverse precursors* ✓ *Easy for large-scale synthesis* ✓ *Great universality for various metals*	✓ *Outstanding conductivity* ✓ *Large specific surface area* ✓ *2D structure*	✓ *Well-defined pore structures* ✓ *Controllable shape and size of MOFs-derived carbon matrix* ✓ *Variable metal nodes and organic linkers*
✗ *Less controllable* ✗ *Hard to precisely regulate the coordination environment*	✗ *Low metal loading* ✗ *Time-consuming graphene synthesis process*	✗ *Complicated synthesis process* ✗ *Poor universality*

Figure 9. Comparison of three kinds of SACs for CO_2RR.

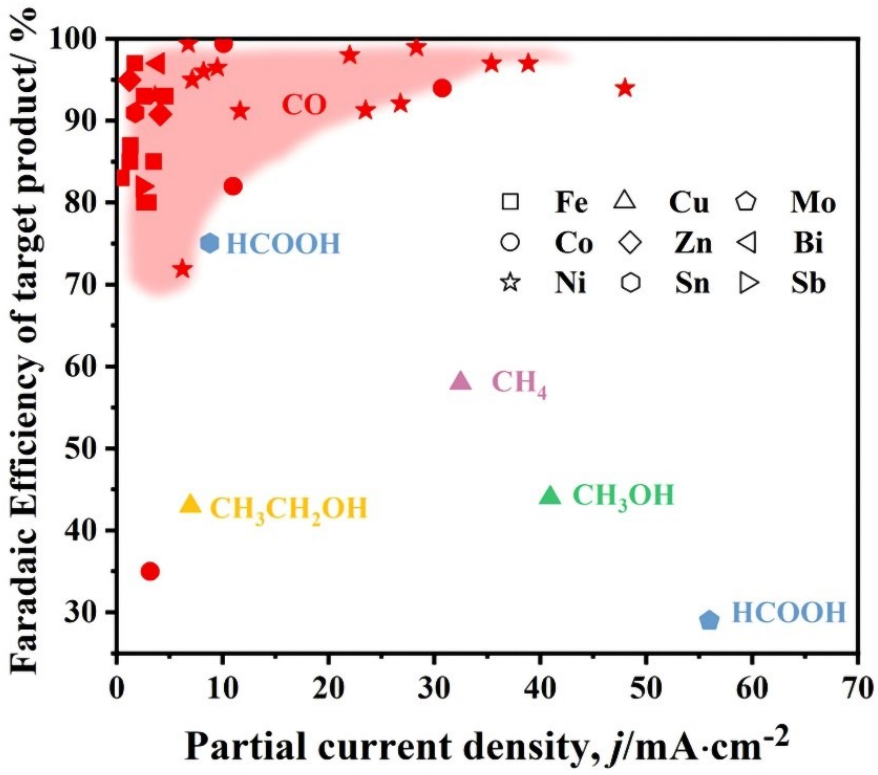

Figure 10. Summary of CO_2RR performance of SACs. The CO_2RR performance reported on various SACs in the H-cell.

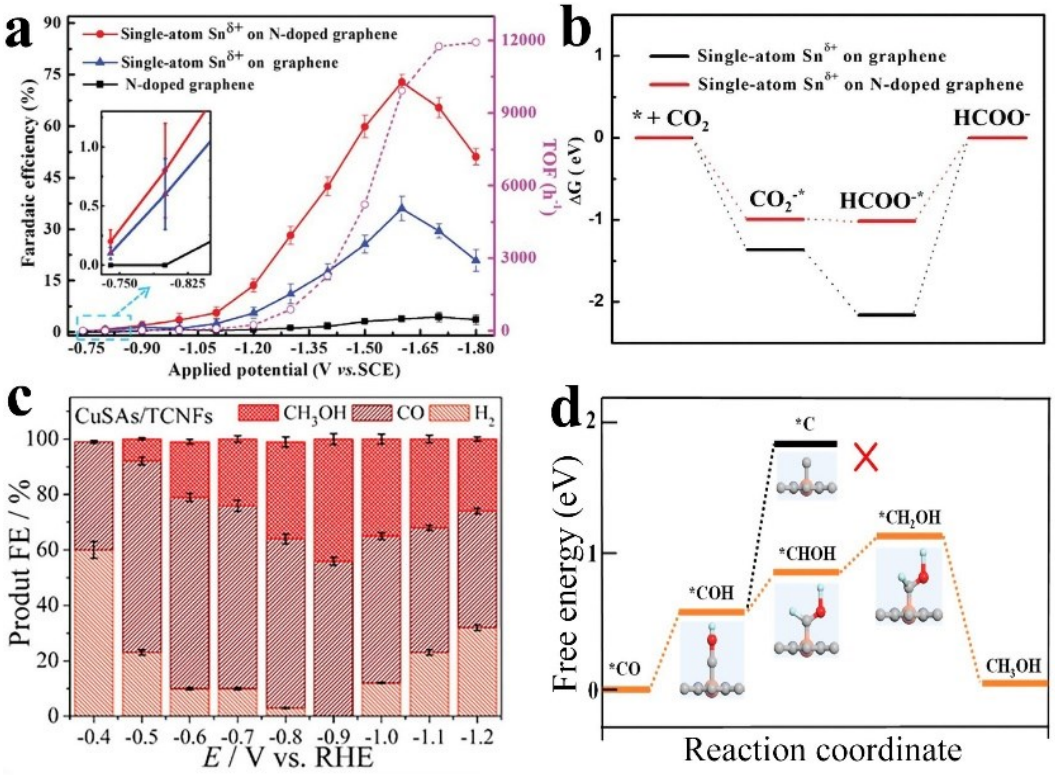

Figure 11. CO_2RR products beyond CO on SACs. (a) and (b) CO_2RR to formate over single-atom $Sn^{\delta+}$ on N-doped graphene. Reproduced with permission.[76] Copyright 2019, Wiley-VCH. (c) and (d) CO_2RR to methanol over CuSAs/TCNFs. Reproduced with permission.[188] Copyright 2019, American Chemical Society.

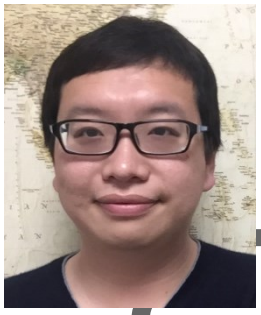

Wei Luo is a Professor in the State Key Laboratory for Modification of Chemical Fibers and Polymer Materials, College of Materials Science and Engineering at Donghua University. He obtained the Bachelor (2006) and Master (2009) degree at Nanjing Tech University (China). He received his PhD. in chemistry in 2014 from Fudan University supervised by Professor Dongyuan Zhao. His research interests mainly include the functional mesoporous materials and structural ceramics.

Jun Chen is a Full Professor, Head of Postgraduate Studies, at Intelligent Polymer Research Institute (IPRI) | ARC Centre of Excellence for Electromaterials Science (ACES), Australian Institute for Innovative Materials (AIIM), University of Wollongong (UOW). He received his Bachelor degree (1995) at Zhejiang University of Technology (China) and PhD degree (2003) at University of Wollongong (Australia). His research interests include: sustainable energy devices/systems, electro-/bio-interfaces, nano/micro-materials, 2D/3D printing, and design and fabrication of smart electronic devices.

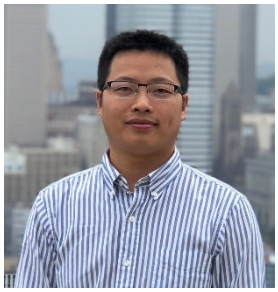

Jianping Yang is a full professor in the College of Materials Science and Engineering at Donghua University, China. He received his Bachelor degree (2007) at Huazhong University of Science and Technology. His Master (2010) and PhD degree (2013) were received from Fudan University supervised by Professor Dongyuan Zhao. He then worked as a postdoctoral and visiting research fellow at Tongji University, University of Wollongong and Monash University. His research interests focus on spatially confined design of environment-friendly materials for environmental remediation, electrocatalytic denitrification, energy conversion and storage (including Si-based lithium ion batteries, carbon-based sodium/potassium ion batteries).

Heterogeneous single-atom catalysts exhibit promising performance for electrochemical CO_2 reduction reaction. Various valuable reduction products have been produced on different single-atom catalysts. In these catalysts, single atomic sites coordinate with heteroatoms, such as N and S, and locate in N-doped carbon materials, graphene, or MOFs-derived carbon frameworks.

Keyword: CO_2 reduction reaction, electrocatalyst, single-atom catalysts, N-doped carbon, metal-nitrogen sites

Minhan Li, Haifeng Wang, Wei Luo*, Peter C. Sherrell, Jun Chen* and Jianping Yang*

Heterogeneous Single-atom Catalysts for Electrochemical CO_2 Reduction Reaction